Small-Angle X-Ray Scattering Studies of Microvoids in Amorphous-Silicon-Based Semiconductors

Final Subcontract Report
1 February 1991 – 31 January 1994

D. L. Williamson, S. J. Jones, Y. Chen
Colorado School of Mines
Golden, Colorado

NREL technical monitor: W. Luft

◆NREL

MASTER

NOTICE

Printed on recycled paper

DISCLAIMER

Portions of this document may be illegible
electronic image products. Images are
produced from the best available original
document.

1. EXECUTIVE SUMMARY

1.1 OBJECTIVES

Our general objectives during this three-year research project were to provide new details of the microstructure for the size scale from about 1 to 30 nm in high-quality a-Si:H and related alloys prepared by current state-of-the-art deposition methods as well as by new and emerging deposition technologies and thereby help determine the role of microvoids and other density fluctuations in controlling the opto-electronic properties.

More specifically, the objectives were to determine whether the presence of microstructure as detected by small-angle x-ray scattering (SAXS) (1) limits the photovoltaic properties of device-quality a-Si:H, (2) plays a role in determining the photo-stability of a-Si:H, and (3) is responsible for degradation of the photovoltaic properties due to alloying with Ge, C and other constituents. The approach involved collaboration with several groups that supplied relevant systematic sets of samples and the associated opto-electronic data to help address these issues. Since the SAXS technique had not been a standard characterization technique for thin-film materials, and was set up at CSM with support by NREL, an underlying 4th objective of the project involved considerable development of the method with regard to identifying and interpreting various scattering contributions to the signals in the small-angle regime, standardizing the procedures, minimizing substrate influences and implementing improved data reduction and modeling methodology. Precise, highly reproducible, and accurate results were sought in order to allow useful, reliable, and sensitive comparisons of materials deposited under different conditions, by different methods, and by different systems that represent the same nominal method.

1.2 CONCLUSIONS

The SAXS technique as developed during this project is able to provide microstructural information not available from other methods and with a high degree of sensitivity. It is particularly sensitive to microvoids or H-rich microdomains and to the presence of oriented microstructure. The latter is readily associated with columnar-type growth and can even be observed in premature stages not detectable by transmission electron microscopy (TEM). New results related to alloy randomness have emerged from our ability to measure the diffuse scattering component of the SAXS. Flotation density measurements provided important complementary data. Specific conclusions from our three-year research program under NREL support are presented below relative to each of the three primary objectives as well as the fourth objective related to

interpretation and development of the technique:

1) Role of SAXS-detected microstructure in photovoltaic properties of a-Si:H

(a) Extremely low microvoid volume fractions of the the order of 0.1% or less have now been established in films grown by a few groups, all by the PECVD method but with different conditions. All of these films show high-quality photovoltaic or opto-electronic behavior.

(b) a-Si:H p-i-n solar cells that contain more microstructure in the i-layer in the form of spherical or randomly-oriented microvoids and more H bonded as Si-H_2 show lower initial efficiencies.

(c) Dilution during 70 MHz PECVD growth with Ar causes enhanced microstructure in the form of microvoids. High Ar dilution leads to a highly oriented microstructure consistent with columnar-like growth. This behavior correlates with opto-electronic degradation. He dilution during PECVD growth allows increased deposition rates and reduced substrate temperatures while maintaining a low microvoid content and little or no oriented microstructure. Low defect densities and high photoconductivities are obtained in these He-diluted films. Although several ECR-produced films were made with and without Xe dilution, too many other parameters were varied to allow a conclusion on the effect of the Xe.

(d) Alternative deposition methods including hot-wire, ECR and RMS all yield a-Si:H films that show significant microvoid volume fractions (1 to 2%) and yet high photo/dark conductivity ratios ($\sim 10^5$) are observed. However solar cells have not yet been fabricated with these alternate deposition methods. Also, we have not yet obtained hot-wire material with the low H contents that show improved light stability.

2) Role of SAXS-detected microstructure in the photostability of a-Si:H

(a) a-Si:H p-i-n solar cells that contain more microstructure in the i-layer in the form of very small voids and more H bonded as Si-H_2 show more light-induced degradation. These results are in disagreement with suggestions by a Japanese group that more microstructure may yield more stable material.

(b) No change in SAXS could be detected after accelerated light-soaking of several a-Si:H films, thereby demonstrating that the Staebler-Wronski instability does not induce detectable changes in the microstructure such as void size increases or larger amounts of H within the voids. This result is not unexpected since the maximum number of defects involved in this important electronic effect is of the order of $10^{17}/cm^3$. However, the microvoids or H-rich domains, as detected by SAXS, are at least this dense and therefore may play a direct role as the source of H or the location of

the weak Si-H bonds, proposed to be responsible for the light instability.

3) Role of SAXS-detected microstructure in the photovoltaic properties of alloys

(a) a-$Si_{1-x}Ge_x$:H alloys that show a microstructural transition corresponding to enhanced columnar-like growth above $x=0.2$ have corresponding sharp degradations in opto-electronic properties above this same Ge content. This provides strong evidence that the increased low-density heterogeniety is directly responsible for the degradation.

(b) Solar cells made from a-$Si_{1-x}Ge_x$:H alloys have efficiencies that decrease smoothly with increasing x and SAXS from the corresponding alloys show little change in the microstructure until the Ge contents reach 31 and 41 at.%. Thus, an obvious correlation of SAXS and initial cell efficiencies was not found. However, the cell light-soaking stability was noticeably poorer for the latter two Ge contents.

(c) Angle-independent, random alloy (diffuse) scattering from a-$Si_{1-x}Ge_x$:H alloys has been observed and identified. for the first time. A theoretical quadratic x dependence is in good agreement with the observed dependence of the data on x but the magnitude of the effect is much too strong. This enhanced diffuse scattering is direct evidence of short-range clustering of Ge and this effect may play an important role in the opto-electronic degradation due to short-range potential fluctuations.

(d) The SAXS-determined microstructures of a-Ge:H PECVD films prepared with variable electrode spacing and variable plasma power are the most homogeneous for those films with the best opto-electronic properties. a-Ge:H without oriented microstructure has not yet been observed for PECVD films but it has for sputter-deposited films. Ge-rich a-$Si_{1-x}Ge_x$:H alloys ($x \simeq 0.7$) have recently been produced at Harvard University that show SAXS signals approaching the best a-Si:H.

(e) a-$Si_{1-x}Ge_x$:H:F alloys prepared by PECVD from silane and germanium fluoride are microstructurally different from all the other PECVD alloys in that a larger fraction of smaller scattering centers are present in a more randomly oriented array. Typically, this non-columnar-like microstructure yields better optoelectronic properties (see (a) above).

(f) A set of PECVD a-SiC:H alloys from Solarex shows strong SAXS due to microvoids that are so dense that they are correlated in position as evidenced by an interparticle interference effect in the SAXS curves. Such a microstructure is a likely limitation on the opto-electronic properties that are clearly in need of improvement.

(g) a-SiC:H alloys prepared by RMS all have a higher degree of oriented microstructure in contrast with PECVD materials which have randomly oriented or spherical microvoids. The RMS material has lower amounts of SAXS-detected

microstructure and higher film densities for similar C contents. The average void size is smaller in the PECVD films.

(h) A first set of B-doped a-Si:H and a-SiC:H samples indicates small but systematic increases in the SAXS due to increased doping concentrations.

(i) Another approach to high bandgap material is being tested via Se alloying and a set of samples containing up to 7 at.% Se (corresponding to a Tauc gap increase of 0.09 eV) shows little change in the SAXS relative to a-Si:H and no evidence of Se clustering.

4) SAXS interpretation and methodology:

(a) An absolute calibration of the integrated SAXS signal for two-phase systems has been made based on theory and experiment. Experiments were made with four model two-phase systems: AlAg and CuBe alloys, Sb_2O_3 particles, and CdTe quantum dots. Theory and experiment agree within 15%. The expected SAXS signal due to a given volume fraction of voids can be predicted on the basis of a two-phase microstructure consisting of voids of zero density in a hydrogenated amorphous matrix. A void fraction as low as 0.1% can be detected for films of 1 μm thickness on a high-purity Al-foil substrate. The calibration work has also allowed our SAXS intensities to be converted to standard units (electron units) that now allows comparison to other results and to theoretical predictions, typically made in terms of these units.

(b) Identification of several scattering mechanisms that can contribute to the SAXS, in addition to the standard electron density fluctuations such as microvoids, has been made and substantiated by theory. These include Laue monotonic scattering due to alloy diffuse scattering, thermal diffuse scattering due to atomic vibrations, static disorder diffuse scattering due to the amorphous structure, and incoherent Compton scattering. The intensity due to all of these mechanisms can be calculated in electron units and compared to experimental data. The most important of these is the alloy scattering effect and new information on the atomic-scale microstructure can be obtained via this effect. It is crucial to correct for these diffuse scattering mechanisms, all angle-independent or nearly so, in analyzing the SAXS data for microvoid contents, particularly for the weak-scattering, higher-quality materials.

(c) The contributions of H alloying and microvoids to the density deficits, as determined by flotation density measurements, can be separated on the basis of an atomic volume for H that is 40% that of Si.

(d) Flotation densities of a-$Si_{1-x}Ge_x$:H alloys for x up to 0.57 show a systematically increasing density deficit (reaching 6%) compared to crystalline densities for samples prepared in 5 different PECVD systems. Coexistence of Ge-rich or Si-rich regions in

these films cannot yet be ruled out but the evidence presented here strongly supports the void (or low density H-rich domain) interpretation. There are differences in the degree of oriented-type microstructure for a similar x in films from different systems.

(e) Modeling of the sample tilting effects on the SAXS intensities due to oriented scattering centers is possible on the basis of a distribution of ellipsoidal voids. Values of the major/minor axis ratio can be estimated for the tilt data.

(f) Carefully designed experiments have established that interdiffusion is negligible between the aluminum foil substrate (used to prepare the films for SAXS) and the a-Si:H provided that substrate temperatures are no higher than 400°C. Temperatures below 350°C should be used for films containing Ge.

(g) A high sensitivity of SAXS to microcrystallinity in a-Si:H based films has been established with μc-Si films and with a-Si:H films annealed above 400°C where microcrystalline regions develop. Integrated SAXS signals a factor more than 100 larger than device-quality a-Si:H are observed.

TABLE OF CONTENTS

2. INTRODUCTION

The term "microstructure" is a rather general one in materials science used to describe structural features that range in size depending on the structural probe. This term is most often associated with structural features observed directly with optical and electron microscopes where images with resolution from micrometers to nanometers are obtained. A recent, relevant example is the TEM observation of hydrogen-induced platelets in crystalline silicon which are only about 1 atomic layer thick but many nanometers in diameter[1,2]. Unfortunately, amorphous materials, such as the a-Si:H-based solar cell films of interest here, yield relatively poor contrast with these conventional techniques unless they are extremely inhomogeneous and therefore typically of poor opto-electronic quality. Device-quality a-Si:H and a-SiGe:H appear homogeneous by TEM[3,4]. Spectroscopic methods such as electron spin resonance, infrared spectroscopy (IR), nuclear magnetic resonance (NMR), Raman, and positron-annihilation are less direct microstructural probes but they are able to provide atomic-scale structural information that often improves our understanding of the connection between structure and opto-electronic behavior. In some cases such as IR[5], NMR[6], and positron-annihilation[7], larger-scale features such as microvoids or H clusters can be inferred. Non-random alloying effects that may be associated with either segregation or ordering can be deduced from Raman spectroscopy based on counting the type and fractions of the nearest-neighbor bonds[8]. Simple mass-density measurements using film flotation methods[9,10] provide rather direct support for inhomogeneous, low-density material but yield no specific information on its microstructural nature.

During the last few years we have been applying a direct structural technique based on the diffraction of x-rays to determine quantitatively some aspects of the microstructure of a-Si:H and the related alloys, a-SiGe:H and a-SiC:H. This somewhat uncommon technique, small-angle x-ray scattering (SAXS), has proven to be a powerful and valuable probe. Our general objectives were to provide new details of the microstructure for the size scale from about 1 to 30 nm in high-quality a-Si:H and related alloys prepared by current state-of-the-art deposition methods as well as by new and emerging deposition technologies and thereby to help determine the role of microvoids and other density fluctuations in controlling the opto-electronic properties.

Results which support the conclusions listed in the Executive Summary for a-Si:H, a-SiGe:H and a-SiC:H are described in detail. In addition, a summary discussion is presented of the very different microstuctures existing in current state-of the art a-Si:H, a-SiGe:H, and a-SiC:H.

1

3. EXPERIMENTAL METHODS

X-ray intensity scattered at an angle 2θ relative to the incident beam passing through a sample is obtained with a highly collimated beam formed by a Kratky block collimation system[11]. The angle 2θ is usually converted into the magnitude of the momentum transfer during scattering, $h=(4\pi/\lambda)\sin\theta \simeq (2\pi/\lambda)2\theta$, and the x-ray intensity is collected in units of photons/s in a step-scan mode for a prescribed set of h's and times at each h. A sample consists of a film deposited onto a thin Al-foil substrate that can be folded to produce multiple layers and enhanced signals. A few films have been co-deposited onto thin c-Si wafers for comparison. The measured x-ray intensity is corrected for substrate scattering and absorption effects, and normalized for variations in film thickness and incident intensity[12] to yield what we call the normalized SAXS intensity, I(h). Experimental data can be displayed as lnI(h) versus h as shown in Fig. 1 for several a-SiGe:H alloys together with a set of data from a c-Si wafer for reference. Note in this figure that each set of data approaches an apparent constant level at high h and that this level depends on the Ge content. We now understand this behavior as due to diffuse scattering from at least two mechanisms (Laue monotonic scattering[13] and disorder scattering). The data must be corrected for this effect by subtraction of the constant level of scattering in order to further analyze the remaining SAXS due to true microstructure effects. Further discussion of this effect and results from our consideration of possible substrate/film interdiffusion effects are discussed below in the "SAXS interpretation and methodology" section.

After correction for the diffuse scattering effect, a useful method of displaying data is to plot the product hI(h) versus h as shown in Fig. 2a for a set of a-Si:H films, since, under the assumption of a two-phase, randomly-oriented microstructure, the area under such a curve is directly proportional to the volume fraction of the minor phase[14]. This area, $\int I(h)hdh=Q$, represents the reduction of a set of SAXS data to a single number that can be used to quantitatively compare the microstructures of various samples. If an oriented microstructure is present then the SAXS and the resulting Q may be strongly affected and the direct proportionality with volume fraction is no longer valid. However, this case can be readily detected by tilting the sample relative to the x-ray beam and monitoring the changes in I(h) and Q. We have found it convenient to simply compare the Q obtained at 0° tilt angle compared to that at 45° in the form of the ratio Q(0°)/Q(45°). Figure 2b shows an example of such tilting data for two samples of a-Si:H. A ratio of unity demonstrates no oriented microstructure, while values greater than unity suggest elongated scattering centers with their long axes preferentially

parallel to the growth direction similar to columnar-type microstructure. A ratio below unity would be consistent with plate-like scattering centers preferentially oriented with their large axes in the film plane.
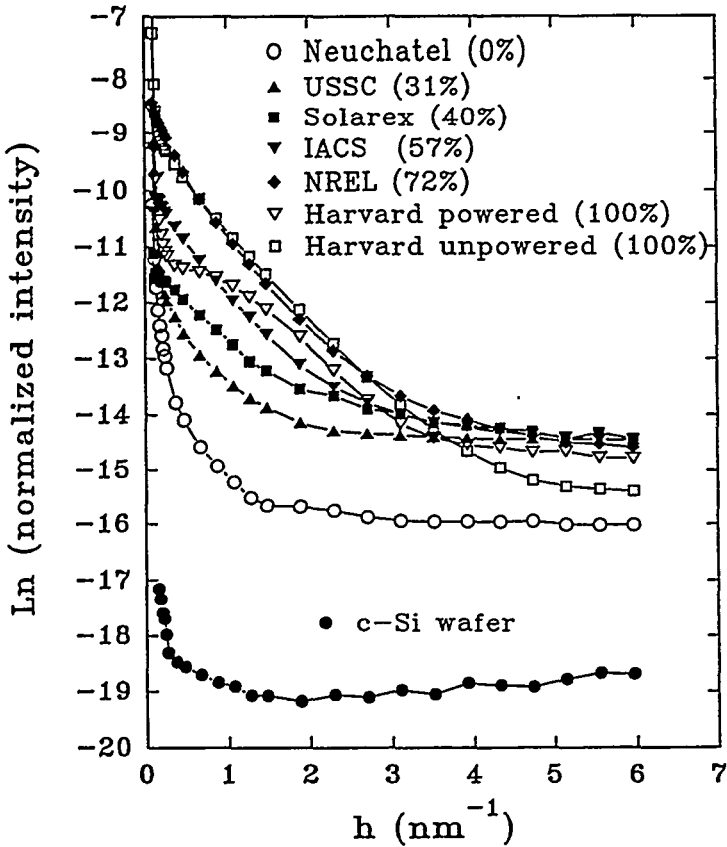
Fig. 1. Typical SAXS data for a-SiGe:H alloys (Ge at.% in parentheses). Also shown are reference data from a c-Si wafer and data from a high-quality a-Si:H film.
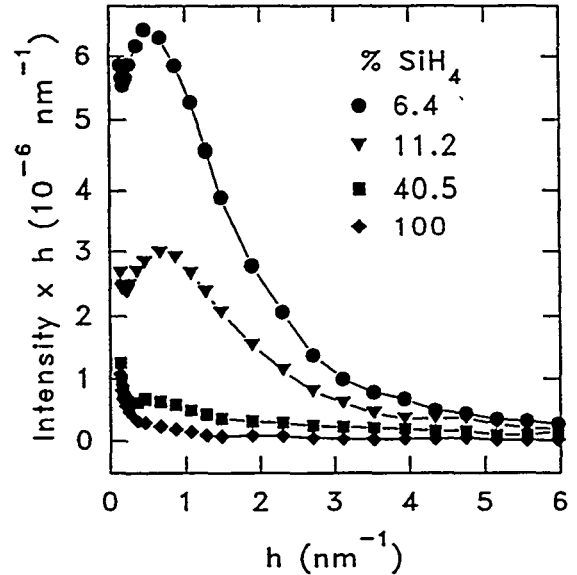
Fig. 2a. Ixh plots for a set of a-Si:H films prepared by 70 MHz PECVD under Ar dilution
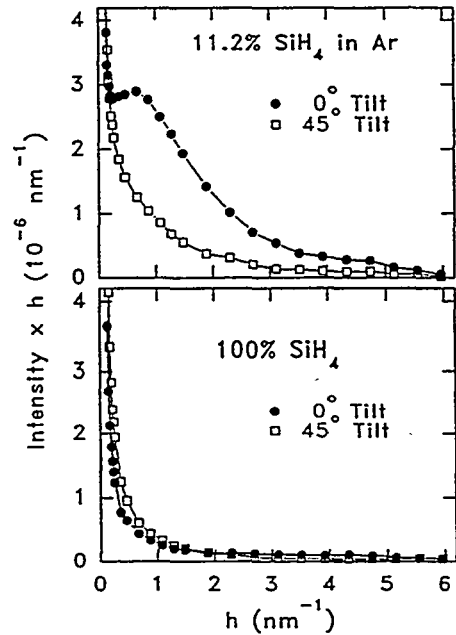
Fig. 2b. Tilting data for two of the samples of Fig. 2a.

3

4. RESULTS AND DISCUSSION

4.1 SAXS from a-Si:H

We have made SAXS and flotation density measurements of numerous a-Si:H thin films prepared by rf glow-discharge (PECVD), hotwire filament (HW), remote hydrogen plasma (RHP), reactive dc magnetron sputtering (RMS), and electron cyclotron resonance (ECR). Several of these samples can be characterized as "device quality" on the basis of their photoresponse and other opto-electronic properties. Deposition variables that were systematically varied included plasma power (primarily to change deposition rate), use of diluting gases (H_2, Ar, He, and Xe), and substrate temperature. Suppliers of a-Si:H films produced by the various deposition methods included: PECVD - NREL, USSC, APS, Solarex, Ecole Polytechnique (Paris), Utrecht University, Stuttgart University, and the Indian Association for the Cultivation of Science (IACS); high-frequency PECVD - Univ. Neuchatel; HW-NREL; RHP-Xerox; RMS - University of Illinois; and ECR - JPL and Iowa State University.

A correlation of SAXS-determined microstructure and solar cell behavior has been obtained and reported[15]. A series of SAXS samples and solar cells were prepared by USSC with different deposition rates used for growth of the i-layer. This was done by adjusting the rf power of the glow-discharge plasma. The increased microstructure in the form of microvoids about 1 nm in diameter, indicated by the values of Q, correlated with degraded solar cell efficiencies as summarized in Fig.3 for the two extremes in deposition rate. Note that the solar cells with i-layers having the increased microvoid contents degraded more rapidly under light soaking for 600 hours. The increased microstructure was shown not to be associated with an oriented or columnar-like microstructure[15].

Fig. 3. Correlation of SAXS with initial and degraded solar cell efficiencies

4
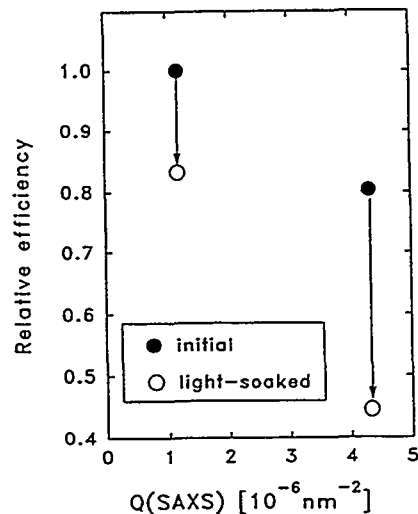
During the first year of this project, five device quality a-Si:H samples were measured in an annealed state (170°C for 20 h) and in an accelerated light-soaked state (20 suns for 20 h). For each of the five films, the SAXS data taken in the two states were the same within experimental uncertainty. To improve the accuracy, one film was first measured in the light-soaked state and then left mounted in the SAXS sample holder for external annealing (170°C for 44 h). It was then reinserted in the SAXS system in the identical position and remeasured. The two sets of data are practically identical[16]. Based on these results we conclude that there is no change in the SAXS-detected microstructure due to the Staebler-Wronski effect. This result is *not unexpected* since (i) the structural changes which may accompany light soaking/annealing are small in magnitude and generally thought to be confined to an atomic scale associated with breaking/healing of weak Si-Si or Si-H bonds such that defect densities of about $10^{17}cm^{-3}$ are involved; (ii) the SAXS method is insensitive to hydrogen due to weak x-ray scattering from its one electron per atom. However, the microvoids or H-rich domains, as detected by SAXS, are at least this dense and therefore may play a direct role as the source of H or the location of the weak bonds.

Several of the other a-Si:H samples produced by the various methods and under certain conditions showed a significant amount of SAXS-determined microstructure that correlated systematically with deposition variables and degraded opto-electronic behavior:

(a) The use of a larger amount of Ar dilution during 70 MHz PECVD deposition caused clear increases in Q and this was accompanied by a lowering of the photoconductivity, a broadening of the Urbach edge and an increase in sub-bangap absorption[17]. A clear transition to oriented, columnar-like microstructure was induced by the Ar dilution.

(b) He dilution of a standard 13.56 MHz plasma, coupled with an increase in substrate temperature from 250 to 320°C allowed an increase in deposition rate to 1.2 nm/s with Q values and opto-electronic properties typical of device-quality material[17]. The scattering centers produced in the He dilution study were significantly smaller than those of the Ar dilution study and there was less tendency for an oriented microstructure.

(c) The deposition of a-Si:H at high rates by the cathode heating technique[18] has yielded a correlation SAXS-determined microstructure and powder formation in the plasma due to gas-phase polymerization[19]. Enhanced void fractions and poorer initial and light-soaked photoresponse were observed for the films grown under dusty plasma conditions.

For other a-Si:H deposition methods [Hotwire[20], ECR[21] and RMS[22]] a significant

5

amount of SAXS-detected microstructure was present and yet photo/dark conductivity ratios typical of device-quality material were obtained. However, none of these materials were incorporated as i-layers into solar cells to evaluate their device performance. Films from APS and Solarex that represent their current state-of-the-art a-Si:H used as the i-layer in their best solar cells have been studied and the SAXS Q-values are among the lowest yet observed. The remote hydrogen plasma (RHP) method developed at Xerox also yields quite low SAXS.

For convienient comparison of the SAXS from a-Si:H deposited by various groups and by the various methods, data are listed in Table 1 and several complete sets of SAXS data are plotted in Fig. 4, where the variability in angular dependence and intensity is due to different size distributions and volume fractions of scattering centers in the various a-Si:H films, respectively. The samples from each group that yield the lowest SAXS Q-values are included along with the known deposition conditions and known opto-electronic properties. Assuming that only voids are responsible for the listed Q's, the maximum possible void volume fractions can be calculated on the basis of the approximate expression V_f(in %) $\simeq Q/4x10^{-6}nm^{-2}$ (this is not exact because it depends on the H content bonded in the matrix). Flotation densities and total bonded H contents (via IR) are listed as well.

Examination of the data in Table 1 reveals that several samples have maximum void fractions that are less than 0.1% and that are approaching our detection limit with the SAXS system of about 0.03%. In fact, these best quality samples may contain less voids than indicated since the Q obtained from these samples is predominantly due to scattering at low h (see Fig. 4) which corresponds to some larger-scale microstructural features that are not likely to be voids. To explore more carefully this smaller-angle scattering, some experiments were made on two of the high-quality films using a narrower entrance slit of 42 μm vs our standard slit of 130 μm. The two samples examined had different thicknesses of about 1 and 10 μm so that the possibility of surface roughness could be tested as one origin of the small-h signals. However, as shown in Fig. 5 the normalized data are quite similar in magnitude, suggesting a bulk mechanism. (However, these two films were grown by different groups and a more careful study of a possible surface roughness effect is needed). The log-log plot of Fig. 5 yields a slope near that of the Porod law of -3 showing that we are probably seeing only the tails of the scattering curves caused by structural features that must be larger than about 30 nm in size. One can estimate whether H concentration fluctuations of on this size scale could be the source of the SAXS. For example, if one considers the a-Si:H

6

Group	Deposition method	Preparation details	Q_0 $(10^{-6}nm^{-2})$ (thickness)	Q_0/Q_{45}	L_A $(x10^{-7})$	C_H (at %)	ρ_{flot} (g/cm^3)	Opto-electronic properties
APS #B751	PECVD	200°C; 1 sccm; H-dilu 0.15mbar; 10mW	0.3 (3.0 μm)	1.0	0.8	~7	2.24	cell efficiency 8 % (stabilized)
Ecole poly #304144	PECVD	60% He dilu; 350°C; 1.12nm/s	0.3 (4.7 μm)	1.0	0.9	9.2	2.23	Nd(PDS):~1x10^{16}cm^{-3}; R=0.05; E$_0$=49meV; σ_{photo}=6.6x10^{-7} (ohm*cm)$^{-1}$
IACS #CH33	PECVD	180°C; 20sccm 0.32nm/s; H-dilu	1.4 (6.4 μm)	1.7	1.9	15.5	2.18	R=0.33
Illinois #1780T	RMS	0.16mTorr P$_{H2}$ 230°C;	2.1 (2.4 μm)	1.5	0.5	9.2	2.26	R=0.05; Eg=1.71eV; $\sigma_{photo}/\sigma_{dark}$=2.0x10^3 Eo=51meV; Nd(PDS):~1.6x10^{16}cm^{-3}
Iowa State #1/386	ECR	---	1.2 (0.9 μm)	---	---	---	---	---
JPL #20115B	ECR	350°C; 20sccm; 300W Xe 15sccm; 1.0mTorr	1.8 (1.2 μm)	1.0	0.5	---	2.23	$\sigma_{photo}/\sigma_{dark}$=2.8x10^6
Neuchatel #170293	VHF-PECVD	70MHz; 0.22 mbar 9W; 300°C; 40sccm	0.1 (3.2 μm)	0.9	0.5	9.6	2.24	R=0.1;Eg=1.69eV $\sigma_{photo}/\sigma_{dark}$= ~2.0x10^5
NREL #128	hot wire	300°C;20sccm; 7mTorr; 1nm/s	3.0 (2.9 μm)	1.7	1.3	12.0	2.18	Eg=1.71eV; $\eta\mu\tau$=1.2x10^{-8}(cm^{2}V^{-1}) Eo=51meV; $\sigma_{photo}/\sigma_{dark}$=3.0x10^5
NREL #A9/12/90	PECVD	300°C	0.6 (1.7 μm)	0.9	0.5	7.5	---	Eg=1.65eV; $\eta\mu\tau$=2.0x10^{-6}(cm^{2}V^{-1}) Eo=49meV; Nd(PDS):~7x10^{15}cm^{-3}
Princeton #M280	PECVD	---	1.1 (1.0 μm)	1.2	1.9	---	---	Eg=1.75eV; $\sigma_{photo}/\sigma_{dark}$=3.8x10^5 Eo=52meV; Nd(CPM):~9x10^{15}cm^{-3}
Stuttgart #205251	PECVD	200°C; 30sccm; H-dilu 0.34mbar; 50mW/cm^2	0.8 (2.5 μm)	1.0	0.5	7.7	---	Eo=56meV;Eg=1.72eV, $\sigma_{photo}/\sigma_{dark}$=3.6x10^4 Nd(PDS):~2x10^{16}cm^{-3}
USSC #4810	PECVD	0.14nm/s; 300°C	1.2 (0.9 μm)	1.0	0.9	8.0	2.24	R=0.08; cell efficiency: 7.85% (initial) & 6.53% (stabilized)
Utrecht #A422	PECVD	200°C; 30sccm 10W; 0.12mbar	1.1 (1.3 μm)	1.0	1.4	12.0	2.20	R=0.13; Eg=1 71eV
Xerox #444	RHP	400°C; 400W; H-dilu 10sccm; 0.5mTorr	0.4 (2.3 μm)	1.0	0.6	~10	2.21	Eo=50meV; Nd(PDS):~3x10^{15}cm^{-3}

C_H: bonded H content (via IR);

ρ_{flot}: film density via flotation method;

N_d: defect density;

E_0: Urbach energy;

σ: conductivity;

E_g: Tauc gap;

$\eta\mu\tau$: quantum efficiency, mobility, lifetime product

R: I(2080)/[I(2000)+I(2080)], where I is integrated IR intensity

7
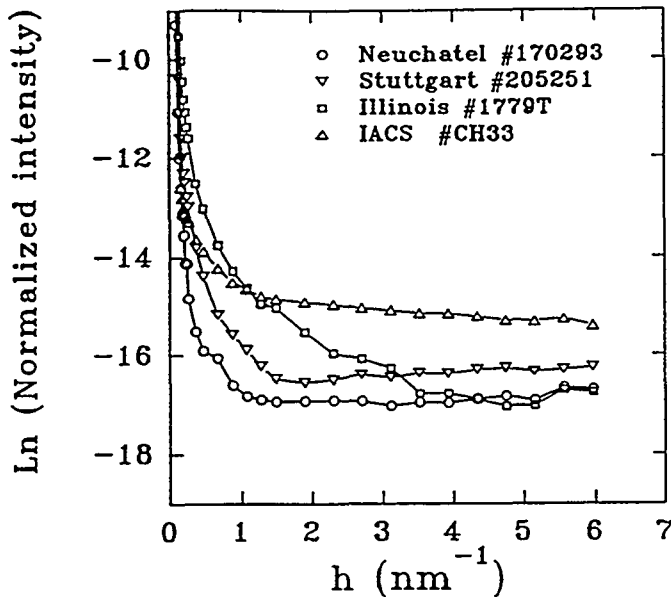
Fig. 4. SAXS scans from some of
the samples listed in Table 1.
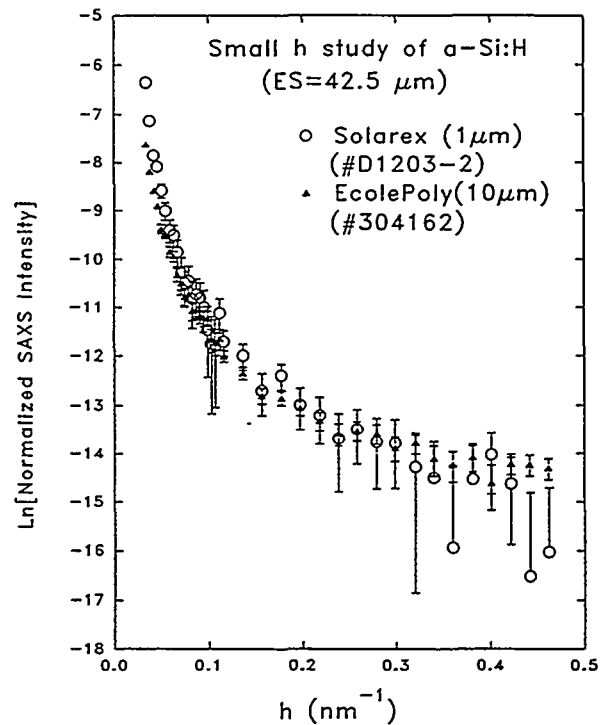
Fig. 5. SAXS at low h for thick (10 μm)
vs. thin (1μm) a-Si:H films.

matrix as a two-phase system with some fraction, f, of its volume with a 10 at.% H content (bonded in the matrix) and the other fraction, 1-f, at 10+δ at.% H, then one can calculate that the expected $Q \simeq 0.0065\delta^2 f(1-f) \times 10^{-6} nm^{-2}$ (i.e., in the same normalized intensity units of Table 1). Since the maximum possible value of f(1-f)=0.25 and most of the Q will not be detected experimentally due to their large size, we can safely write $Q(max)=0.0016\delta^2 \times 10^{-6} nm^{-2}$. Thus, even δ=3% will cause a Q that is about an order-of-magnitude below the lowest values in Table 1 so that this type of mechanism does not appear feasible. Further work is needed to clarify the origin of this low-angle, weak, but perhaps significant SAXS.

4.2 SAXS from a-SiGe:H

Several sets of a-SiGe:H alloys from various groups have been analyzed. These include PECVD films from NREL, Solarex, USSC, Stuttgart University, Harvard University, IACS, and Princeton University. The latter samples were prepared with GeF_4 rather than GeH_4. Some of the SAXS data from these samples as well as data from Harvard a-Ge:H films were compared in Fig. 1 together with a typical device-quality a-Si:H sample and our reference crystalline-Si data. An initial investigation of several a-SiGe:H alloy films[23] has now been supplemented by more extensive and systematic studies as described below.

A systematic series of 10 samples from Stuttgart University with Ge contents from 0 to 37 at.% provide strong evidence for a direct link between the SAXS-determined microstructure and opto-electronic degradation[24]. Above about 20 at.% Ge a sharp transition in the microstructure occurs consistent with a change to columnar-like growth. As shown in Fig. 6, above this same composition the photo/dark conductivity ratio and the defect density determined by photothermal deflection spectroscopy (PDS) show significant decreases and increases, respectively.

A comparison of the Q's from the Stuttgart samples with those from alloys made by the other groups is shown in Fig. 7. There is apparently an ubiquitous problem in the microstructure of a-SiGe:H alloys with Ge content above 20-30 at.%. These same high concentrations also lead to $Q(0°)/Q(45°)$ ratios in the range from 2 to 5 indicating strongly oriented microstructures[21]. Flotation densities from all a-$Si_{1-x}Ge_x$:H films with x below 0.6 (the density limit of our fluid) are shown in Fig. 8 in comparison with the density of crystalline alloys[25]. A quadratic fit to the data and the resulting difference from the crystalline alloys is shown in the lower plot of Fig. 8. Note that the density deficit reaches 6%, consistent with an interpretation of voids or low density, H-rich regions as the source of the SAXS. The H content generally decreases with increasing Ge, so the increased deficit cannot be attributed to H in the matrix. Japanese researchers have been suggesting that alloy segregation (Ge-clusters) is the origin of the SAXS in a-SiGe:H alloys[26,27].

Additional evidence that such large-scale Ge clustering is not responsible for the SAXS comes from measurements of several a-Ge:H films prepared by PECVD at Harvard. The SAXS signals are quite similar to those from the SiGe alloys (Fig. 1) but, of course, no Ge clustering can be present in such material, except relative to the H and voids, which is our interpretation of the origin of the SAXS. Further details of SAXS studies of a-Ge:H films is presented later.
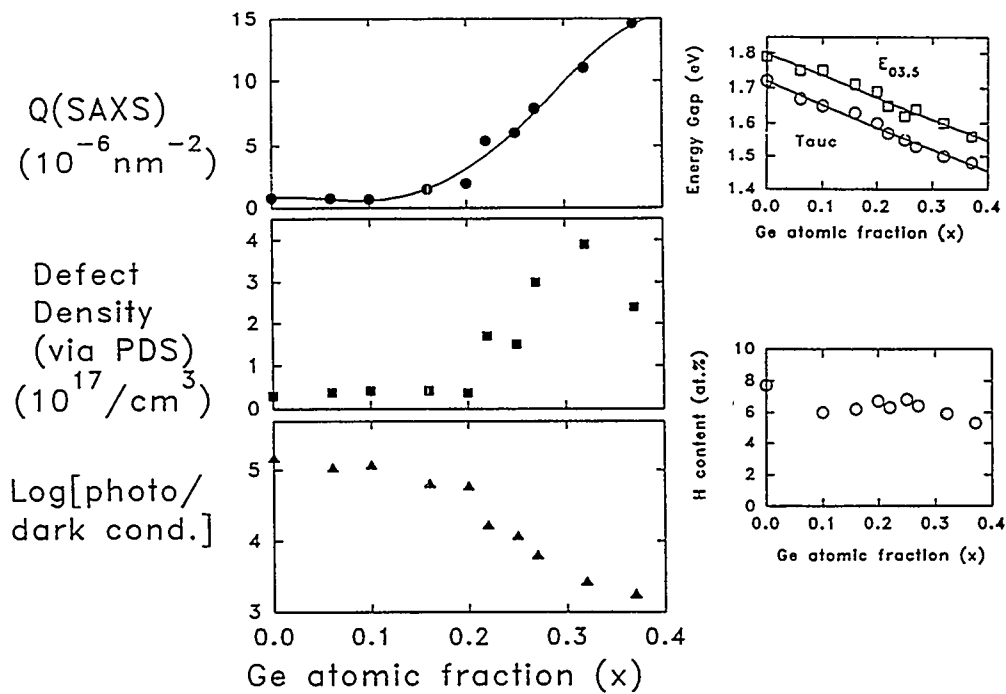
Fig. 6. Correlation of SAXS and opto-electronic properties of a-SiGe:H alloy films prepared at Stuttgart Univ. (from ref. 23). Also shown are the bandgaps and bonded H contents versus Ge content.
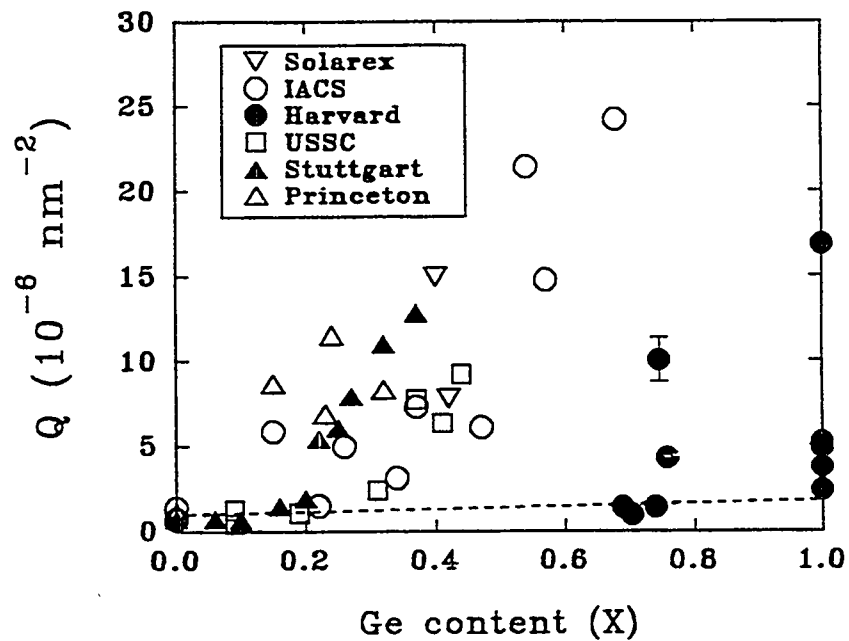
Fig. 7. Comparison of integrated SAXS intensities from a-SiGe:H alloys prepared by PECVD by several groups.
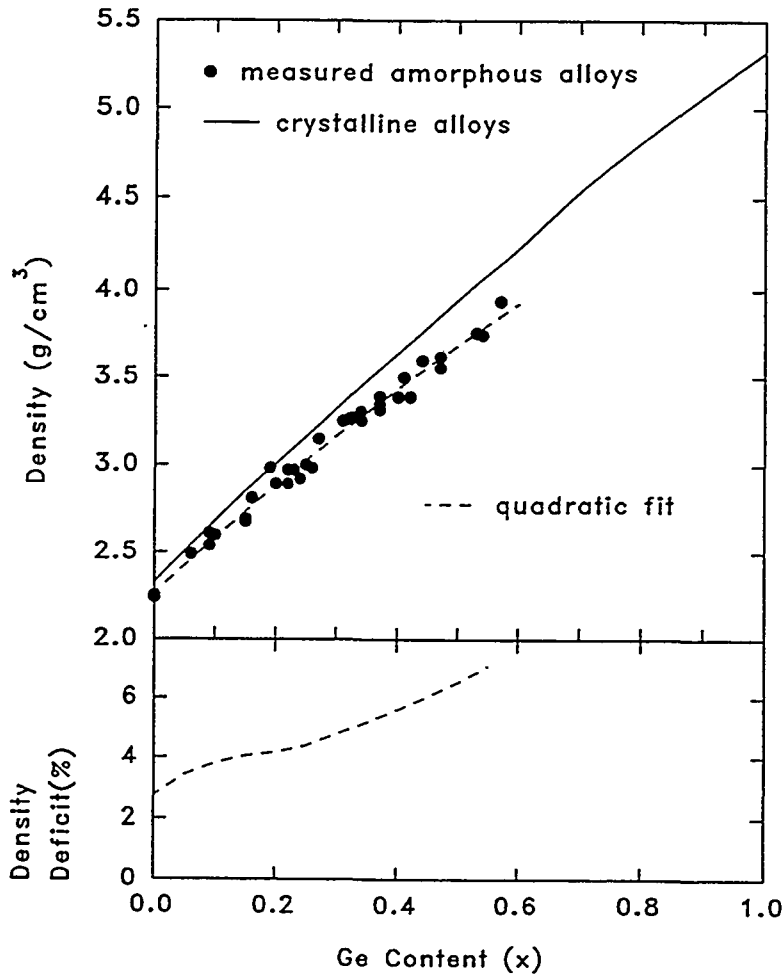
Fig. 8. Flotation densities of a-$Si_{1-x}Ge_x$:H compared to crystalline $Si_{1-x}Ge_x$ alloys.

A USSC series of alloys (included in Fig. 4) shows a similar trend to that of the Stuttgart series in that oriented microstructure appears for the 31 and 41% Ge films, although the magnitudes of the increases in Q are not as great, suggesting more homogeneous microstructure than the Stuttgart films for similar Ge content. Solar cells containing i-layers made under identical deposition conditions used for the SAXS samples show systematically reduced initial efficiencies with increasing Ge while the Q's do not increase significantly until the above Ge contents are reached. However, increased light-induced degradation was observed for these two higher Ge content solar cells. Details of this study have been reported[28]. Further research is needed to understand the role of SAXS-detected microstructure in film opto-electronic properties versus photovoltaic properties. The direction of carrier transport relative to the film plane may be important in cases where oriented microstructure is present[28].

11

The Princeton material, prepared with GeF_4, suggests a significantly different size distribution of scattering centers and a reduced tendency for columnar-like microstructure. Thus, the source gas can have a strong effect on the microstructural character of the film.

Recent Ge-rich a-SiGe:H alloys prepared at Harvard by PECVD on the powered electrode (cathode) are of particular interest due to a sharp improvement in opto-electronic properties for such high Ge films and a corresponding sharp reduction in SAXS-detected microstructure. These results are included in Fig. 7 where one can see the low Q's for x near 0.7, clearly much lower than most of the values from samples with $0.2 < x < 0.6$. Table 2 lists the deposition conditions, opto-electronic properties, and SAXS results for these new samples. Note that the values of $Q(0°)/Q(45°)$ are near unity so that the oriented type of microstructure has essentially been eliminated. Such results suggest that modified deposition conditions could also lead to elimination of the significant microstructural inhomogeniety remaining in the lower Ge-content material of interest for the low bandgap i-layer of a multijunction cell, $x \simeq 0.4\text{-}0.5$.

Table 2. Preparation conditions, opto-electronic properties, and SAXS results from PECVD a-SiGe:H alloys prepared at Harvard University.

SAXS sample	Corre-sponding sample	Deposition conditions * $H_2 : SiH_4 : GeH_4 \ /\ D$ (cm)	E_{04} (eV)	E_{03} (eV)	C_{GeH} (at.%)	C_{SiH} (at.%)	$C_{H,tot}$ (at.%)	GR (Å s^{-1})	$\eta\mu\tau$ ($cm^2 s^{-1}$)	E_{act} (eV)	L_0 (Å)	stress (kbar)
395	415	40 : 1.0 : 1.0 / 1.0	1.57	1.39	4.5	15.6	20.1	9.59	3.0e-8	0.64	598	-5.4
401	398	40 : 0.5 : 1.0 / 1.0	1.40	1.25	5.4	5.5	10.9	7.76	9.3e-8	0.59	494	-4.9
404	403	40 : 0.3 : 1.0 / 1.0	1.36	1.21	5.7	6.5	12.2	6.79	1.6e-7	0.58	552	-6.2
416	NA	40 : 1.0 : 1.0 / 1.2										
418	417	60 : 1.0 : 1.0 / 1.0	1.56	1.39	6.6	12.1	18.7	7.78	9.8e-8	0.67	527	-5.9
420	419	80 : 1.0 : 1.0 / 1.0	1.52	1.34	6.1	10.2	16.3	6.74	3.5e-8		481	-5.6
422	421	20 : 1.0 : 1.0 / 1.0	1.52	1.33	3.5	14.0	17.5	13.3	6.1e-8	0.65	517	-5.7
423	415	40 : 1.0 : 1.0 / 1.0	1.57	1.39	4.5	15.6	20.1	9.59	3.0e-8	0.64	598	-5.9

* All other deposition conditions were the same: 225 °C, 30 Watts, 0.95 Torr, powered electrode.

Sample	X_{Ge} (at.%)	Q_0 (10^{-6} nm^{-2})	Q_0/Q_{45}	I_A (10^{-7})	Thickness (μm)
#395	72.0	2.8	0.7	3.9	0.7
#401	84.0	19	2.4	2.5	0.6
#404	86.0	13	—	3.3	3.0
#416	74.0	1.4	0.9	5.3	5.0
#418	75.8	4.3	1.0	5.7	3.6
#420	74.6	10	1.5	5.2	3.9
#422	68.9	1.4	0.9	4.6	3.6
#423	70.4	1.0	0.9	4.8	4.2

4.3 SAXS from a-SiC:H

Figures 9 and 10 compare the SAXS intensity scans and microstructure quantity Q for several samples of a-SiC:H films prepared by reactive dc magnetron sputtering[22], RMS, at the Univ. of Illinois and by PECVD at Solarex. Although methane was the source of the C in both cases, there are significant differences in microstructure. All of the RMS films show a significant tilting effect such that $Q(0°)/Q(45°)$ is 1.3-1.6 while the PECVD material yields ratios of 0.9-1.2 (only one was above 1.1). Thus, oriented microstructure exists in the RMS material while more random orientations exists in the PECVD films. Also, the I(h) data in Fig. 9 show quite different behavior with h for the two types of deposition, suggesting a quite narrow distribution of 1 nm diameter scattering centers in the PECVD material and a wider distribution of somewhat larger scattering centers in the RMS films. One may compare the Q's in Figs. 7 and 10 to see that C incorporation of less than 20 at.% leads to much more microstructure, in contrast to Ge alloying. ·

The appearance of a shoulder-like pattern in the SAXS of the PECVD films (Fig. 9) indicates an interparticle interference effect. Generally, there are two criteria that need to be met for the occurrence of this effect[11]: (i) a high density of scattering centers and (ii) a rather narrow size distribution. Earlier results from PECVD a-SiC:H alloys prepared at NREL[12,29] also showed the shoulder-like feature in the SAXS and there it was proposed that the high density of CH_3 groups as detected by IR could be responsible for the high density of very small microvoids. No such interference features have yet been detected in any a-Si:H or a-SiGe:H films.
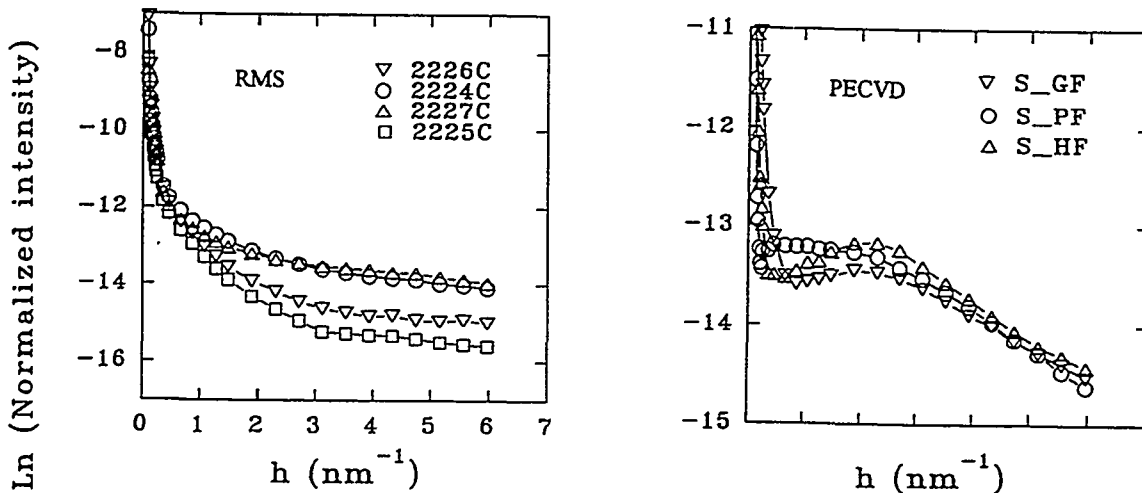
Fig. 9. SAXS scans from RMS and PECVD a-SiC:H alloys.
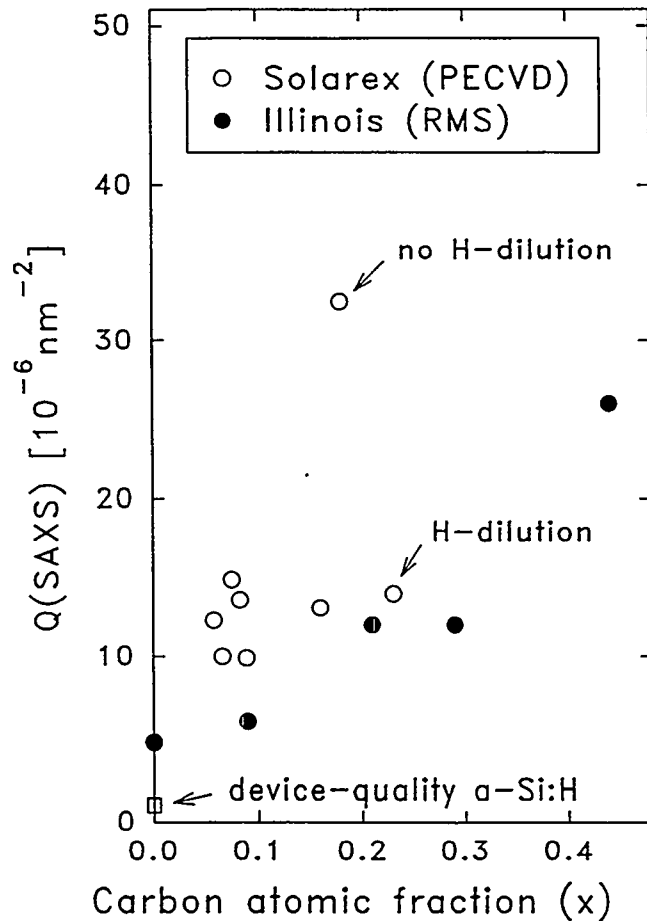
Fig. 10. Comparison of integrated SAXS intensities from a-SiC:H alloys prepared by two methods.

Table 3 summarizes all currently known information about the a-SiC:H alloys prepared by the two methods. Note the significantly smaller densities of the PECVD films for similar C content. The last six Solarex samples is the series of samples prepared as part of the NREL High-gap Team effort. Opto-electronic properties were supplied by two team members (Univ. of Illinois and Penn State) and both sets of data are included for comparison.

Table 3. Comparison of properties of a-SiC:H prepared by RMS vs PECVD.

Sample	T_s (°C)	Xc	C_H (at.%)	Eg (eV)	Urbach Eo (meV)	σ_{photo} + (Ω cm)$^{-1}$	$\mu\tau$ (cm²/V s)	DOS(CPM) (10^{15}cm^{-3})	ρ_{flot} (g/cm³)	Q # (10^{-6} nm^{-2})	Q_0/Q_{45}
•2225C	275	0.0	13	1.67	48	1.4×10^{-6}	--	1.2	2.22	4.6	1.6
•2226C	275	0.09	14	1.71	53	1.0×10^{-6}	--	6.3	2.17	5.9	1.2
•2224C	275	0.21	24	1.90	66	3.5×10^{-7}	--	10	2.08	12.0	1.3
•2227C	275	0.29	25	1.95	71	5.2×10^{-8}	--	27	2.10	12.0	1.4
••S PF	265	0.10	--	⁻1.95	80	--	$<6\times10^{-10}$	--	2.03	15.7	1.1
••S GF	265	0.16	--	⁻1.95	>110	--	1×10^{-8}	--	2.06	13.1	1.1
••S QF	250	0.18	--	⁻1.95	79	--	1×10^{-9}	--	1.92	32.5	1.0
••S HF	180	0.23	--	⁻1.95	69	--	4×10^{-8}	--	2.05	14.0	1.2
••A3018-1	--	0.01	12.8	1.8	64	2.4×10^{-6}	5.3×10^{-7}	160	2.18	575	0.9
••A3006-1	--	0.09	16	1.9	50	7.1×10^{-7}	1.6×10^{-7}	4.8	2.10	9.9	1.1
••A3019-2	--	0.06	14.6	1.95	63	1.4×10^{-7}	2.8×10^{-8}	170	1.98	12.3	1.0
••A3068-1	--	0.08	--	1.95	--	⁻2×10^{-6}	--	--	2.00	13.6	1.1
••A3068-2	--	0.08	23	1.9	--	⁻2×10^{-4}	--	--	2.03	14.9	1.1
••A3005-1	--	0.07	18	1.9	--	⁻1×10^{-6}	--	--	2.11	10.0	1.1

* RMS film; ** PECVD film; + σ_{dark} were all below 4×10^{-12} (ohm cm)$^{-1}$ for RMS films; $\mu\tau$ were from σ_{photo}

\# no correction of alloy scattering due to lack of angle-independent behavior at high h.

note: , the opto-electronic properties listed above for 'A' series samples were provided by Illinois Univ.

Sample	E_{03} (eV)	E_{TAUC}(eV) 2.0-2.4 eV	E_{TAUC}(eV) 2.3-2.6 eV	E_{Cody}(eV) 2.7-3.1 eV	Eo (meV) annealed	Eo (meV) saturated	α (1.2eV) (cm)$^{-1}$ annealed	α (1.2eV) (cm)$^{-1}$ saturated	σ_{photo} + (Ω cm)$^{-1}$	$\mu\tau$ (cm²/V)
A3018-1	1.74	1.81	1.86	1.77	64	72	1.84	32.8	2.4×10^{-6}	1.62×10^{-7}
A3006-1	1.84	1.85	1.94	1.88	50	56	0.10	6.9	7.1×10^{-7}	5.25×10^{-7}
A3019-2	1.94	1.92	2.02	1.92	63	70	0.62	12.5	1.4×10^{-7}	2.75×10^{-8}

note: the opto-electronic properties listed above for 'A' series samples were provided by Pennsylvania state Univ.

4.4 SAXS from Related Materials

4.4.1 a-Ge:H

Two sets of a-Ge:H films from Harvard were prepared to study the effects of electrode spacing and rf power and significant reductions in the SAXS can be obtained when moderate powers and small spacings are used. Table 4 summarizes the opto-electronic and SAXS characteristics of both sets of films. While Q's for a-Ge:H films prepared under these conditions are only slightly larger than values for device-quality a-Si:H (see the lowest point at x=1 in Fig. 7), there is clear evidence of a small amount of oriented microstructure based on $Q(0°)/Q(45°)=2.2$ and 2.1 for the two lowest Q's in Table 4. Details of this work will be presented elsewhere[30].

We have also examined a set of sputter-deposited a-Ge:H films from the group of B. Schroeder of the University of Kaiserslautern (UKL) in Germany. The a-Ge:H from UKL yields quite low SAXS signals as indicated by the data in Fig. 11 compared to one of the high-quality Harvard samples. However, note that the h-dependence is quite different from that of the Harvard PECVD material, i.e. much stronger intensities are observed at lower h. This suggests larger scattering centers in the UKL material which may not be void-related but perhaps surface roughness-related. The analysis of co-deposited films by the UKL group suggests that Al contamination is quite likely affecting the opto-electronic properties which are listed in Table 5 along with the SAXS results. The poorest quality film is #2851 and it has the largest Q. Note that the lowest Q is quite similar to that of the lowest value from the Harvard material (Table 4).

Table 4. Opto-electronic and SAXS results from Harvard a-Ge:H films.

Sample	Electrode spacing (cm)	Plasma power (W)	Ea (eV)	Eo (meV)	$\eta\mu\tau$ (cm^{2}V^{-1})	σ_p/σ_i	$\alpha_{0.7}$ (PDS) (cm^{-1})	C_H from IR (at.%)	Q_0 (10^{-6} nm^{-2})	Q_0/Q_{45}	I_A (10^{-7})
H-257	3.2	10	0.54	61	2.1×10^{-9}	4.5×10^{-4}	65	3.6	43.3	2.7	1.6
H-258	2.0	10	0.56	54	6.0×10^{-8}	1.0×10^{-2}	34	3.8	3.8	3.5	2.0
H-259	1.2	10	0.58	49	1.4×10^{-7}	3.1×10^{-2}	18.5	3.1	2.4	2.2	1.8
H-340	1.4	12	0.49	50	4.8×10^{-8}	5.8×10^{-3}	13.4	4.4	4.9	1.9	1.6
H-338	1.4	30	0.62	47	3.2×10^{-7}	1.2×10^{-1}	10.3	5.7	5.2	2.3	2.9
H-342	1.4	48	0.59	65	6.5×10^{-8}	9.7×10^{-2}	66	7.7	71.8	2.1	2.8
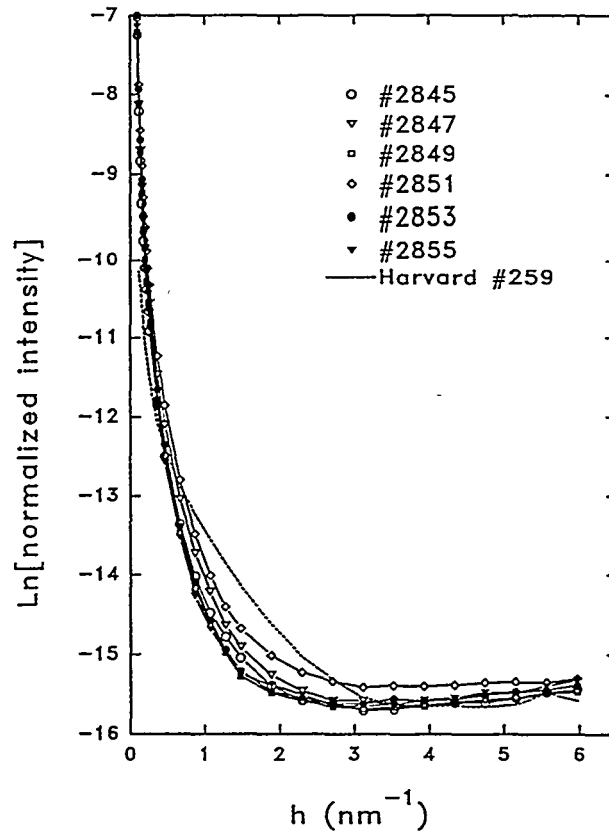
Fig. 11. SAXS from sputter-deposited a-Ge:H prepared at UKL. Data from
the Harvard film prepared with the 1.2 cm electrode spacing is shown
for comparison

Table 5. Opto-electronic and SAXS results from U. Kaiserslautern a-Ge:H films.

Sample	Power (W)	T (°K)	Rate (Å/s)	Ar (mTorr)	H (mTorr)	σ_d (Ω cm)$^{-1}$	C_H (at.%)	E_0 (meV)	Q_0 (10^{-6} nm^{-2})	Q_0/Q_{45}	I_A (10^{-7})	Thickness (μm)
#2845	100	475	5.1	0.9	0.9	3.00E-04	4	45	2.5	1.6	1.3	3.7
#2847	100	475	4.9	1.3	1.3	2.40E-04	4	47	2.9	1.1	1.5	3.5
#2849	100	475	4.6	0.5	0.7	1.40E-02	4.5	44	2.1	1.4	1.5	3.3
#2851	200	475	10.0	0.5	0.7	2.90E-02	4.5	65	3.6	1.2	1.9	3.9
#2853	100	475	4.0	0.5	0.7	1.30E-02	6	48	2.4	1.9	1.6	2.9
#2855	50	475	2.2	0.5	0.5	1.10E-04	4.5	51	2.2	1.5	1.6	3.2

4.4.2 Boron-doped a-Si:H and a-SiC:H

Two sets of boron-doped films have been provided by the group at Utrecht University. They represent our first systematic investigation of doped material. Figure 12 compares samples from the a-Si:H(B) series and the a-SiC:H(B) series to demosntrate the SAXS-detected changes induced by adding B_2H_6 to the PECVD plasma. The ratios given in the figure refer the gas flow ratios of 1% B_2H_6 in H_2/pure SiH_4 (5 sccm, constant). The data show increases in the SAXS due to B incorporation. Table 6 lists the SAXS and flotation data as well as B and C contents determined by electron-probe micro-analysis (EPMA) at NREL. The B contents do not appear systematic with the gas flow ratios and disagree with systematic behavior of other properties such as conductivity activation energy, band-gap, and IR. This is likely due to B contents near the sensitivity limit of the EPMA. The tilting ratios are all unity within experimental error (± 0.1) and this demonstrates no oriented microstructure is present in any of the films.

There are two columns in Table 6 for the flotation density because for the a-Si:H(B) series we were able to obtain values from flakes that were peeling from the glass substrates (ρ_{gl}) as well as from film removed from the Al-foil by acid etching (ρ_{Al}). The consistency of these two sets of numbers (within 0.01 g/cm^3, our experimental uncertainty in this method), is a good indication of little difference in the films co-deposited on glass and the SAXS Al-foil. As can be seen the densities are dramatically lower than those of diamond-like $Si_{1-x}C_x$ (about 2.6 g/cm^3 for x=0.27) [or for graphitic-like SiC (about 2.3 g/cm^3 for x=0.27)]. Assuming a simple two-phase microstructure of voids plus the amorphous matrix, the size of the Q's in the SiC alloys ($\sim 70 \times 10^{-6}$nm^{-2}) is consistent with void volume fractions near 15-20%. The total bonded H content are not yet available. Further details of this study will be presented by our collaborators[31].

4.4.3 Microcrystalline Si:H

The group at the Univ. of Illinois supplied a few samples of microcrystalline (μc) Si:H samples for investigation by SAXS. These are our first studies of this type of material. The samples were prepared by RMS and they were checked by x-ray diffraction (XRD) for the presence of the μc state. As shown in Table 7, two of the samples were completely amorphous but the other four showed only the μc state. Also the table shows H contents determined by SIMS analysis and the values remain near 10 at.% in the μc state. Figure 13 shows SAXS curves for one of the μc-Si:H samples where one can see extremely strong signals as well as a decrease in the signals with time (stored in air at room temperature). This instability is associated with oxygen
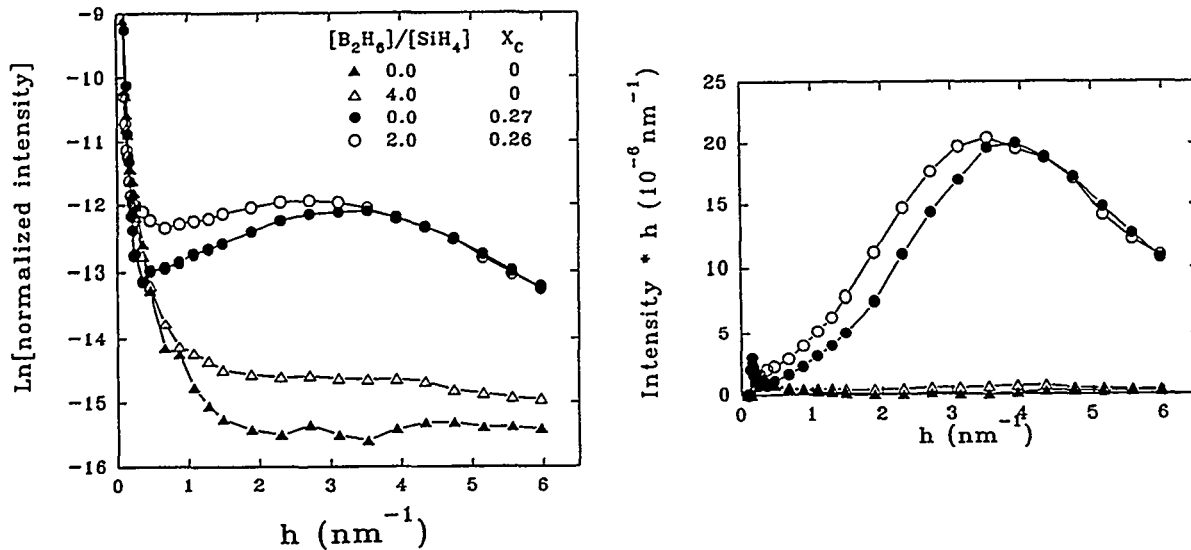
Fig. 12. Effect of B doping on the SAXS of a-Si:H and a-SiC:H films.

Table 6. SAXS, flotation densities and other results for B-doped a-Si:H and a-SiC:H films from Utrecht Univ.

Sample	$B_2H_6 + H_2$ (SCCM)	X_C (at. fraction)	X_B (at. fraction)	t (μm)	Q_o ($10^{-6}nm^{-2}$)	Q_o/Q_{45}	I_{LM} (10^{-7})	ρ_{Al} (g/cm^3)	ρ_{gl} (g/cm^3)
P402	0	0.27	<0.005	0.56	69	1.1 ·	a	1.72	--
P406	0.5	0.27	<0.005	1.28	73	1.1	a	1.70	--
P395	5	0.27	<0.005	1.21	70	1.0	a	1.72	--
P450	10	0.26	0.012	0.65	77	1.1	a	1.76	--
P460	15	0.28	0.003	0.65	67	1.1	a	1.73	--
P455	20	0.25	0.005	0.68	66	1.1	a	1.75	--
P449	0	0	<0.005	0.77	1.3	1.0	1.7	2.19	2.18
P453	5	0	<0.005	0.73	2.5	1.1	2.4	2.17	2.18
P454	10	0	<0.005	0.78	1.6	1.1	2.4	2.16	2.16
P448	20	0	<0.005	0.85	3.0	1.1	2.6	2.14	2.13
P468	0	0	<0.005	1.33	0.7	0.9	1.3	2.23	2.22

a No Laue monotonic background correction was made for these samples.
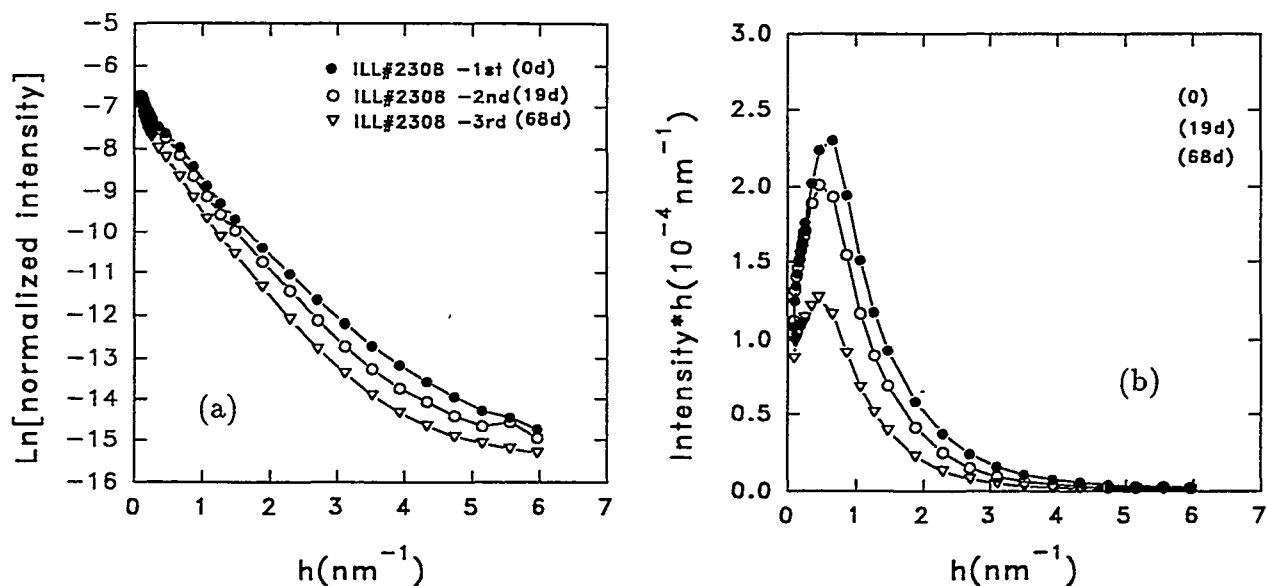
Fig. 13. (a) SAXS intensity from μc-Si:H in the as-received state and after storage in air for increasing times; (b) Ixh plots showing the clear decrease in Q (area under curves) with time.

Table 7. SAXS and flotation density results from μc-Si:H films from Univ. of Illinois.

Sample	H content (at.%)*	Density (g/cm^3)	Q_0 (10^{-6} nm^{-2})	Q_0/Q_{45}	I_A (10^{-7})	XRD	Thickness (μm)
#2297B	~10 %	2.19	490	5.0	—	μc	1.2
#2298B	~10 %	2.13	150	5.4	—	μc	2.0
#2299B	~9 %	2.12	47	2.4	1.22	amorphous	1.6
#2300B	~7 %	2.10	43	2.3	0.98	amorphous	1.4
#2308 (19 days later) (68 days later)	?	2.14	320 260 150	5.4	—	μc	1.7
#2307 (18 days later) (79 days later)	?	2.18	420 380 310	2.7	—	μc	1.4

* SIMS analysis

20

incorporation as detected by IR and by the SIMS analysis. Note that the integrated SAXS intensities as listed in Table 7 are as high as $490 \times 10^{-6} nm^{-2}$, which is about three orders of magnitude larger than typical values for device-quality a-Si:H (see Table 1). Note that this increase occurs without substantial increases in the density deficits, based on the flotation densities shown in the table. Strong tilting effects show that the microstructure is highly oriented so that a columnar-type microstructure is implicated and this probably leads to the post-deposition oxidation. To account for such strong SAXS and the relatively small density deficits requires low-density (and probably heavily hydrogenated) boundaries between the micro-crystallites.

4.4.4 Annealing of a-Si:H

Four samples of a-Si:H prepared by RF sputtering at Iowa State (Shinar's group) have undergone a systematic series of anneals with SAXS and IR carried out after each anneal. The IR measurements were made with films on c-Si substrates (co-deposited with the SAXS films on Al-foil). Annealing at 350°C and above sharply increased the integrated SAXS intensity Q, although the film density remained nearly constant. Incipient formation of μc-Si domains by Si diffusing into the Al substrate is insufficient to account for the increased SAXS. Rather the close correlation between Q and the Si-bonded H content C_H, as shown in Fig. 14, suggests that it more likely results from migration of H released from Si-H bonds to deep traps at microvoid surfaces and its accumulation as H_2 in the isolated voids. The density of the Si network then increases as its H content decreases, and the void sizes increase as hydrogen accumulates in them. The size distributions shown in Fig. 15 are consistent with this interpretation, and consistent with the known characteristics of H diffusion in a-Si:H[32,33].

Annealing for 6 h at 430°C also resulted in some crystallization sufficient to be detected by XRD and Raman spectroscopy. Following 36 h at that temperature, the Raman and XRD indicated that about 50 vol% of the film was still amorphous. Auger profiles showed that Al had diffused throughout the film to a level of 2 to 3 at.%. However an observed reduction in tilt angle dependence is probably not due to filling of the voids by the diffusing Al but rather to the relaxation and reduction of the columnar-like microstructure. Further details of this work are presented elsewhere[34].
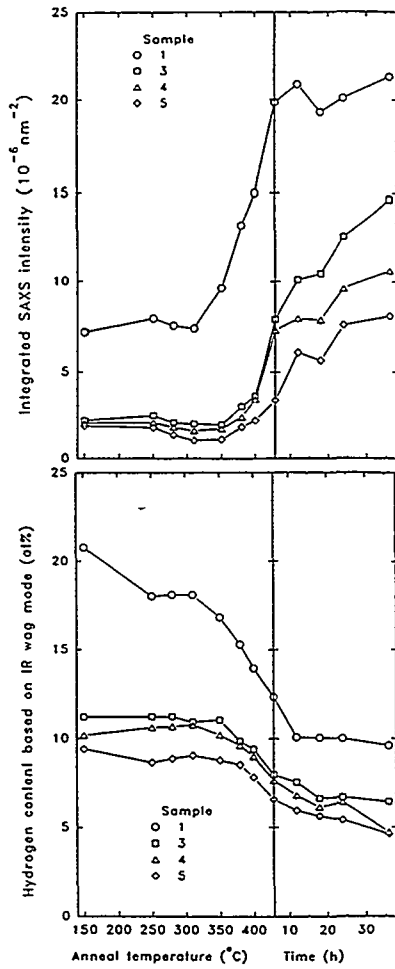
Fig. 14. Integrated SAXS intensities and Si-bonded H contents (from IR) versus annealing temperature and time.
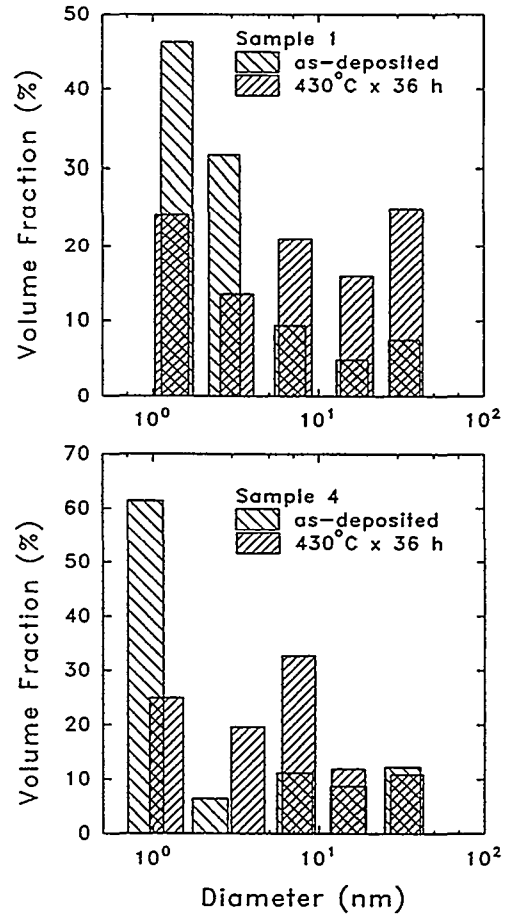
Fig. 15. Distributions of void sizes in samples 1 and 4 before and at the conclusion of the annealing.

4.4.5 a-SiSe:H

A set of seven samples of a-$Si_{1-x}Se_x$:H was prepared by PECVD with silane and H_2Se by the group at Texas A&M Univ. This material is being considered by them (with support by EPRI) as an alternative high-gap material. Table 8 lists the H_2Se flow rates, Se contents, film thicknesses, Tauc band-gaps, conductivities, flotation densities and SAXS results for this set of films. Some of the thicknesses are quite small so there are corresponding large uncertainties in the Q's and I_A's for these films. However, in general the Q's are quite small and several are comparable to the values listed in Table 1 for a-Si:H. There is also no evidence of an oriented microstructure. The sample with the largest band-gap of 1.78 eV, has the poorest photoconductivity but the SAXS is not significantly larger than the other samples, suggesting that other defects are likely responsible for the degradation. It is interesting that that addition of Se does not induce as strong an increase in the SAXS compared to PECVD-prepared a-$Si_{1-x}C_x$:H for similar values of x (see Fig. 10 and Table 3).

22

Table 8. SAXS and other results from a-SiSe:H films from Texas A&M Univ.

Sample	H_2Se sccm	X_{Se} (at.%)	E_g (eV)	$\sigma_{ph}(10^{-5})$ $(\Omega cm)^{-1}$	$\sigma_d (10^{-9})$ $(\Omega cm)^{-1}$	ρ_{flot} (g/cm^3)	Q_o $(10^{-6}nm^{-2})$	Q_o/Q_{4S}	I_A (10^{-7})	Thickness (μm)
Lin#1	0.097	2.78	1.69	2.01	2.41	2.34	0.28	~1	1.0	1.18
Lin#2	0.280	6.34	1.75	0.58	0.59	2.47	0.52	~1	1.2	1.29
Lin#3	0.141	3.85	1.71	1.79	1.47	2.38	3.33	~1	2.8	0.50
Lin#4	0.422	5.83	1.77	0.36	1.10	2.46	0.73	~1	1.9	0.61
Lin#5	0.072	3.41	1.71	5.91	5.64	2.37	4.42	~1	0.9	0.29
Lin#6	0.590	8.03	1.78	0.09	0.77	2.53	0.41	~1	1.6	0.68
Lin#7	0.127	2.97	1.72	2.27	2.39	2.35	0.30	~1	1.2	0.65

4.5 SAXS Interpretation and Methodology

4.5.1 Two-phase microstructure calibration

The integrated intensity, Q, can be converted into a volume fraction of scattering centers under the assumption of a two-phase microstructure provided there is no preferred orientation of the microstructure. For our definition of the normalized intensity[12], I, the conversion of Q to a volume fraction, V_f, can be made from

$$Q= \int h I dh = (\kappa/\mu)(\Delta n)^2 V_f(1-V_f),$$

where Δn is the electron density difference in the two phases of the sample, μ is the linear absorption coefficient of the sample for the x-rays used, and κ is a constant determined by the geometry of the SAXS slit system[35]. For our current geometry the value of κ can be calculated as 1.30×10^{-35} cm^3. We decided to check this value by performing experiments with model two-phase samples where known values of V_f, Δn, and μ could be obtained by careful sample preparation.

Two well-known metallurgical systems that form a two-phase precipitate-matrix microstructure are Al-Ag and Cu-Be. A Cu-Be alloy of known composition (12 at.% Be) was available commercially and an Al-4 at.%Ag was prepared in house. Careful, systematic heat treatments allowed preparation of known volume fractions of precipitates of phases that could be confirmed by XRD: $AlAg_2$ (hcp structure) in Al-Ag and CuBe (cubic CsCl structure) in Cu-Be. In addition, a sample comprised of a known volume fraction of Sb_2O_3 particles in a polymeric matrix was available as a third

standard. The results of the SAXS experiments with these three type of standards are shown in Fig. 16 where theoretical Q's, based on the above value of κ, and the expected values of V_f, Δn, and μ for the samples are compared with the experimental Q's. The solid line with a slope of 45° corresponds to exact agreement and the data are in reasonable agreement with this line. Based on the scatter of the data in this figure and our estimated uncertainties in the theoretical Q's of the standards, the above value of κ has been established within $\pm 15\%$.

The application of this calibration to a two-phase system consisting of microvoids in an amorphous Si-H matrix leads to the prediction that a 1% void fraction in a film with 10 at% H bonded in the matrix will yield a Q of about $4\times10^{-6}nm^{-2}$ (the units used in our tables and plots throughout this document). The predicted values of Q for a void fraction of 1% in a-$Si_{1-x}Ge_x$:H for x=0.5 and x=1 are about 6 and $8\times10^{-6}nm^{-2}$, which are larger due to the effect of larger Δn's. Since we are able to measure a Q as small as $0.1\times10^{-6}nm^{-2}$ for a film of about 3 μm thickness (see Table 1), this demonstrates our ability to detect void fractions as low as about 0.025% in a-Si:H and somewhat smaller in SiGe alloys.
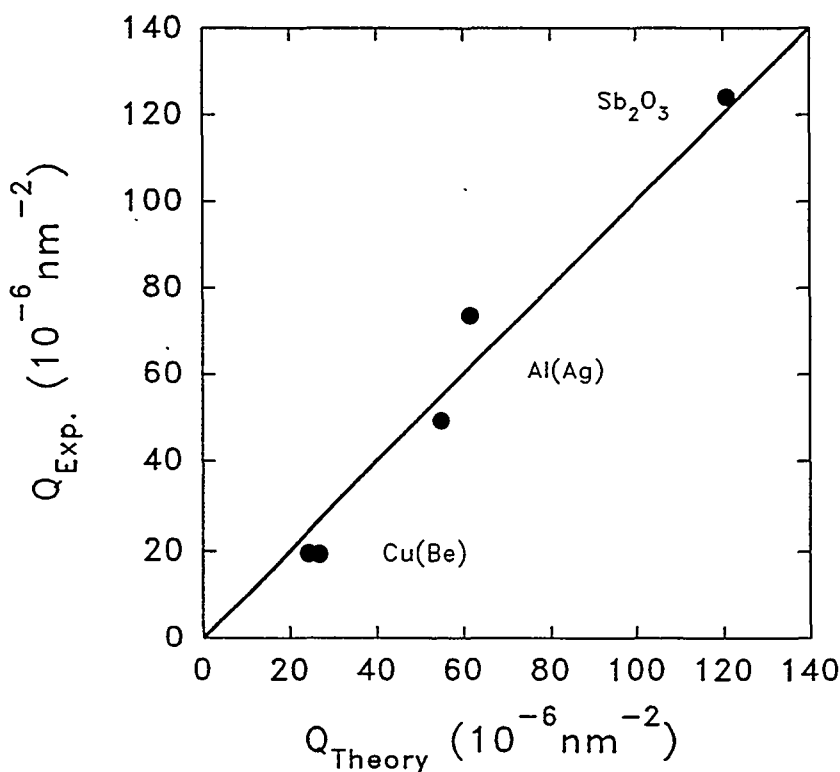

Fig. 16. Comparison of theoretical and experimental SAXS Q's for two-phase calibration samples. The solid line at 45° is that expected for exact agreement between theory and experiment.

4.5.2 Density deficits and H alloying of a-Si:H

It is known that for high-quality c-Si the mass density is 2.3293 g/cm^3. Comparison of the flotation densities in Table 1 with this value shows significant density deficits of several % are present, even in high quality samples with low Q's and, therefore, low void fractions (well below 1%). These deficits have been accounted for with a simple H-alloying model[36] based on several samples with known bonded H contents and known void fractions from SAXS. The only adjustable parameter in the model is the atomic volume occupied by the bonded H atom, Ω_H, expressed as a ratio to that of Si, $\alpha = \Omega_H/\Omega_{Si}$. Results of this analysis are shown in Fig. 17 where one can see a reasonably good fit to the matrix densities assuming $\alpha = 0.4$, i.e. the bonded H occupies only 40% that of a Si atom. Such a value can be shown to be consistent with the much shorter Si-H bond length (0.1480 nm) vs that of Si-Si (0.2352 nm)[36].
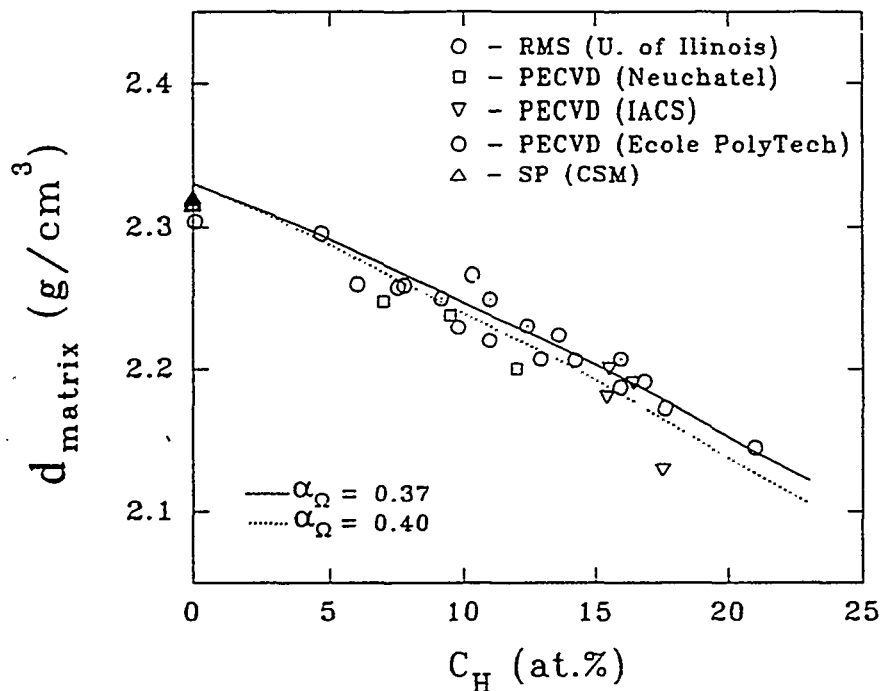

Fig. 17. Matrix densities of a-Si:H films from flotation densities, corrected for small void fractions obtained from SAXS. Solid and dashed lines are fits based on a model with the adjustable parameter α (ref. 36).

4.5.3 SAXS sytem flaw

An experimental problem with the SAXS apparatus was discovered in June, 1992, during a careful examination and adjustment of the system alignment. The cause of the problem was a design flaw in the commercial SAXS system obtained for our research. The flaw was quickly repaired and a systematic study of the effect of the flaw on previous SAXS data was made. The effect of the flaw was to produce an apparent decrease in the SAXS signal with increasing angle above a certain angle. This effect therefore caused errors in the shape of the SAXS curves above this angle. The errors in void fractions and size distributions were relatively small for all samples showing relatively strong SAXS corresponding to void fractions above about 0.5 volume % ($Q \simeq 2 \times 10^{-6} nm^{-2}$), while those for the more weakly scattering material (typically device-quality PECVD films) were larger. The reanalyzed size distributions of the latter type of samples show significantly smaller fractions of the very small voids (about 1 nm diameter), a slight shift in their size toward 2 nm, and a corresponding increase in the fractional contribution from larger scattering centers (about 2 to 3 nm diameter). As discussed in section 4.1 (see Fig. 5), the origin of this larger-scale microstructure is not yet established.

4.5.4 Diffuse scattering contributions

A new feature in most of the SAXS curves that was detected after repair of the flaw is an angle-independent, i.e. diffuse, scattering behavior at the larger angles, as seen in Fig.1, such that constant, but quite different, levels of scattering are found for different samples. In addition, for some of the weakest scattering samples, a slight increase in SAXS with increasing angle at the largest angles was found. Possible physical explanations for these observations have been considered and verified with several experiments[36]. The most important effect that has come to light is that due to random alloy scattering (Laue monotonic scattering[13,14,35]) and it is quite significant for the a-SiGe:H alloys. This effect also produces an observable contribution due to H alloying in a-Si:H. The theory of this effect for a random binary alloy with elements A (atomic fraction x) and B (atomic fraction 1-x) yields the simple result that the diffuse intensity is given (in electron units) by $J_{LM}=x(1-x)(Z_A-Z_B)^2$, where Z is the atomic number. A similar, but more complex expression can be derived for a random ternary alloy, that can be compared to experimental data from a-SiGe:H and a-SiC:H alloys. Theoretical predictions are displayed in Fig. 18 where one can see the relative sizes of the intensities for various alloy compositions, including a-Si:H along the left ordinate.
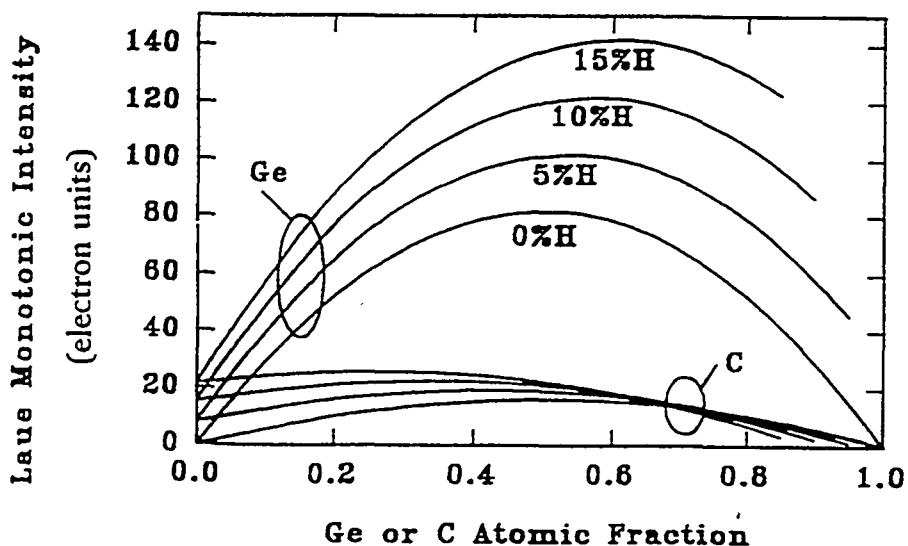
Fig. 18. Theoretical Laue monotonic diffuse scattering contributions for random a-SiGe:H and a-SiC:H alloys with various H contents.

Experimental values of the alloy diffuse scattering, I_A, from about 50 films of a-SiGe:H alloys, including the a-Si:H and a-Ge:H end points are shown in Fig. 19. The solid line is a least-square fit of a quadratic to the data while the dashed line represents the theoretical Laue monotonic scattering for random alloys (converted from the electron units of Fig. 18 to our normalized SAXS intensity units). Clearly, the experimental values are much larger than predicted and this is solid evidence for short-range alloy clustering in this alloy system. Note that there is considerable scatter for several data points near x=0.7, well outside the experimental uncertainty indicated by the error bars. *This suggests that the degree of clustering depends on the deposition process and that it may be controllable.* Evidence of non-random a-SiGe:H alloys has been found by other groups using Raman scattering[37,38].

The diffuse scattering contribution from a-SiC:H alloys prepared by PECVD can not be investigated due to the angle-dependent scattering that occurs up the highest angles (Fig. 9) such that a background level cannot be accurately determined. However, the RMS films do approach well-defined, angle-independent levels (Fig. 9) and the alloy scattering results from these films are shown in Fig. 20. Comparison with the predicted behavior based on random alloying, assuming a H content of 15 at.% (the dashed curve), shows evidence for short-range clustering such that are more Si-Si and C-C bonds than expected for a random alloy. There may be significant contributions also from H clustering associated with non-statistical quantities of C-H_n groups where n=2 and 3. Further correlation with IR data is needed.
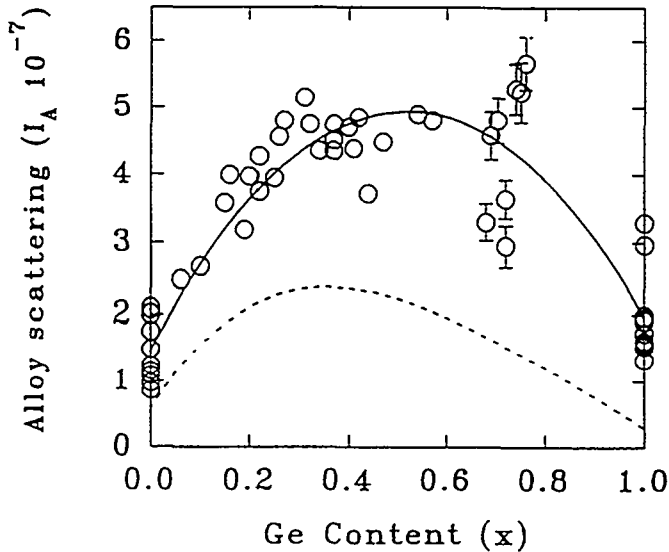
Fig. 19. Diffuse scattering intensities
from a-$Si_{1-x}Ge_x$:H alloys (all prepared
by PECVD).

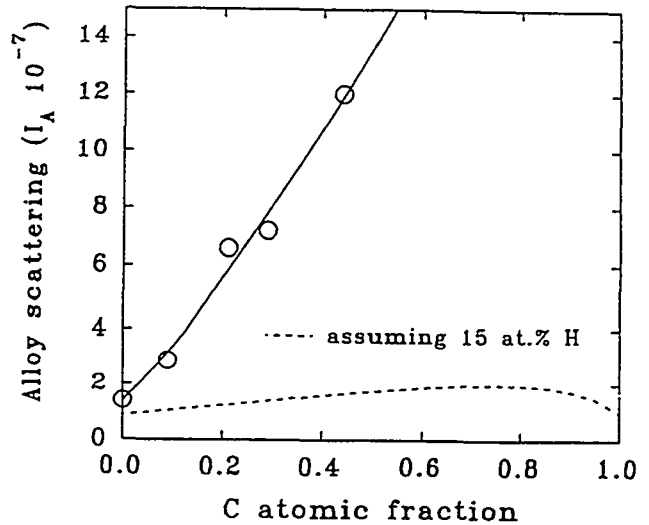Fig. 20. Diffuse scattering intensities
from a-$Si_{1-x}C_x$:H alloys prepared by
reactive magnetron sputtering (RMS).

4.5.5 Substrate/film interdiffusion

A study of the possible interdiffusion between the SAXS Al-foil substrate and a-
Si:H or a-Ge:H films has been completed using depth-profiling Auger electron
spectroscopy[39]. 30-50 nm-thick a-Si:H and a-Ge:H films were deposited onto the Al foil
substrates and annealed at various temperatures up to 600°C. Little or no interdiffusion
was found at or below temperatures of 400°C, contrary to what is typically found by
evaporating Al onto previously deposited a-Si:H films without breaking vacuum, where
interdiffusion occurs at or below 200°C. A native Al-oxide layer about 15 to 30 nm thick
on the Al-foil substrates apparently serves as an effective diffusion barrier until
temperatures of 450-500°C are reached where both interdiffusion and crystallization
occur. The latter was detected by Raman scattering[39].

4.5.6 Modeling of tilting effects

Progress has been made in the modeling of the anisotropic SAXS that is observed
by tilting a sample relative to the x-ray beam. Assuming ellipsoidal-shaped voids, values
of the aspect ratio of the axes can be adjusted for up to five distinct sizes of voids in

order to fit two or more sets of SAXS curves obtained for different tilt angles. Fits to a set of a-Ge:H data suggest aspect ratios in the range from 2 to 6. Details will be presented elsewhere[30].

5. ACKNOWLEDGEMENTS

6. REFERENCES

1. N.M. Johnson, F.A. Ponce, R.A. Street, and R.J. Nemanich, Phys. Rev. B 35, 4166 (1987); N.M. Johnson, Physica B 170, 3 (1991).
2. C.C. Tsai, G.B. Anderson, and R. Thompson, J. Non-Cryst. Solids 137&138, 673 (1991).
3. J.C. Knights and G. Lucovsky, CRC Crit. Rev. Solid State and Mats. Sci. 21, 211 (1980).
4. W. Paul, S.J. Jones, and W.A. Turner, Phil. Mag. B 63, 247 (1991).
5. H. Wagner and W. Beyer, Solid State Commun. 48, 585 (1983).
6. P.C. Taylor, in *Semiconductors and Semimetals,* vol. 21C: *Hydrogenated Amorphous Silicon,* ed. by J.I. Pankove (Academic, Orlando, 1984) p. 99 and references therein.
7. Y.J. He, M. Hasegawa, R. Lee, S. Berko, D. Adler, and A.-L. Jung, Phys. Rev. B 33, 5924 (1986).
8. M.B. Schubert and G.H. Bauer, Phil. Mag. B 62, 59 (1990).
9. P. Menna, A.H. Mahan, and R. Tsu, Proc. 19th IEEE PV Spec. Conf. (IEEE, New York, 1987) p.832.
10. S.J. Jones, Y. Chen, D.L. Williamson, and G.D. Mooney, Mat. Res. Soc. Symp. Proc. 258, 229 (1992).
11. *Small Angle X-ray Scattering,* ed. by O. Glatter and O. Kratky (Academic, New York, 1982).
12. D.L. Williamson, A.H. Mahan, B.P. Nelson, and R.S. Crandall, Appl. Phys.

Lett. **55**, 783 (1989).

13. L.H. Schwartz and J.B. Cohen, *Diffraction from Materials* (Springer-Verlag, Heidelberg, 1987) p.232.

14. A. Guinier and G. Fournet, *Small Angle Scattering of X-rays* (Wiley, New York, 1955).

15. S. Guha, J. Yang, Scott J. Jones, Yan Chen, and D.L. Williamson, Appl. Phys. Lett. **61**, 1444 (1992).

16. D.L. Williamson, Y. Chen, S.J. Jones and G.D. Mooney, Annual Rep., Photovoltaic Subcontract Program FY 1991, NREL/TP-410-4724 (1992) p.18.

17. S.J. Jones, Y. Chen, D.L. Williamson, U. Kroll, and P. Roca i Cabarrocas, J. Non-Cryst. Solids **164-166**, 131 (1993).

18. R. Banerjee, S.N. Sharma, S. Chattopadhyay, A.K. Batabyal and A.K. Barua, J. Appl. Phys. **74**, 4540 (1993).

19. S. Chattopadyay, S.N. Sharma, R. Banerjee, D.M. Bhusari, S.T. Kshirsagar, Yan Chen and D.L. Williamson, (submitted to J. Appl. Phys., 1994)

20. A.H. Mahan, Y. Chen, D.L. Williamson, and G.D. Mooney, J. Non-Cryst. Solids **137&138**, 65 (1991).

21. D.L. Williamson, S.J. Jones and Yan Chen, NREL Second Year Annual Report (1993).

22. Y. Chen, S.J. Jones, D.L. Williamson, S. Yang, N. Maley, and J.R. Abelson, Mat. Res. Soc. Symp. Proc. **258**, 311 (1992).

23. S.J. Jones, Yan Chen, D.L. Williamson and G.D. Mooney, Mat. Res. Soc. Symp. Proc. **258**, 229 (1992).

24. S.J. Jones, Y. Chen, D.L. Williamson, R. Zedlitz, and G. Bauer, Appl. Phys. Lett. **62**, 3267 (1993).

25. J.P. Dismukes, L. Ekstrom and R.J. Paff, J. Phys. Chem. **68**, 3021 (1964).

26. S. Muramatsu, T. Shimada, H. Kajiyama, K. Azuma, T. Watanabe, T. Kamiyama and K. Suzuki, Jpn. J. Appl. Phys. **28**, L1092 (1989).

27. S. Muramatsu, S. Matsubara, T. Watanabe, T. Shimada, T. Kamiyama, and K. Suzuki, J. Non-Cryst. Solids **150**, 163 (1992).

28. S.J. Jones, Y. Chen, D.L. Williamson, X. Xu, J. Yang, and S. Guha, Mat. Res. Soc. Symp. Proc. **297**, 815 (1993).

29. A.H. Mahan B.P. Nelson, R.S. Crandall, and D.L. Williamson, IEEE Trans. Electron Devices **36**, 2859 (1989).

30. S.J. Jones, Y. Chen, D.L. Williamson, P. Wickboldt, D. Pang, A.E. Wetsel, W. Paul and J.H. Chen (in preparation).

31. J. Daey Ouwens, R.E.I. Schropp, W.F. van der Weg and D.L. Williamson submitted to PVSEC, Amsterdam, 1994.

32. J. Kakalios, R.A. Street and W.B. Jackson, Phys. Rev. Lett. 59, 1037 (1987).

33. R. Shinar, J. Shinar, H. Jia and X.-L Wu, Phys. Rev. B 47, 9361 (1993) and references therein.

34. J. Shinar, H. Jia, R. Shinar, Y. Chen and D.L. Williamson, submitted to Phys. Rev. (1994).

35. V. Gerold, in *Small-Angle X-ray Scattering*, ed: H. Brumberger (Gordon and Breach, New York, 1967) p. 277.

36. Yan Chen, Ph.D. Thesis, T-4492, Colorado School of Mines (1994).

37. L. Yang J. Newton and B. Fieselmann, Mat. Res. Soc. Symp. Proc. 149, 497 (1989).

38. M.B. Schubert and G.H. Bauer, Phil. Mag. B 62, 59 (1990).

39. S.J. Jones, A.B. Swartzlander-Franz, Y. Chen and D.L. Williamson, Mat. Res. Soc. Symp. Proc. 297, 1049 (1993).

APPENDIX:

LIST of PUBLICATIONS from this RESEARCH

A. "The structure of a-Si:H by small angle x-ray scattering" A.H. Mahan, Y. Chen, D.L. Williamson and G.D. Mooney, J. Non-Cryst. Solids 137&138, 65 (1991).

B. "Effect of microvoids on initial and light-degraded efficiencies of hydrogenated amorphous silicon alloy solar cells" S. Guha, J. Yang, Scott J. Jones, Yan Chen and D.L. Williamson, Appl. Phys. Lett. 61, 1444 (1992).

C. "Small-angle x-ray scattering from a-Si:H and a-SiC:H alloys prepared by reactive dc magnetron sputtering" Y. Chen, S.J. Jones, D.L. Williamson, S. Yang, N. Maley and J.R. Abelson, Mat. Res. Soc. Symp. Proc. 258, 311 (1992).

D. "Small-angle x-ray scattering studies of glow-discharge-produced a-SiGe:H alloys" Scott J. Jones, Yan Chen, D.L. Williamson and G.D. Mooney, Mat. Res. Soc. Symp. Proc. 258, 229 (1992).

E. "Microstructure transition and degraded opto-electronic properties in amorphous SiGe:H alloys" S.J. Jones, Y. Chen, D.L. Williamson, R. Zedlitz and G. Bauer, Appl. Phys. Lett. 62, 3267 (1993).

F. "Correlation of SAXS and solar cell performance of a-SiGe:H alloys" S.J. Jones, Y. Chen, D.L. Williamson, X. Xu, J. Yang and S. Guha, Mat. Res. Soc. Symp. Proc. **297**, 815 (1993).

G. "Interdiffusion at a-Ge:H/Al and a-Si:H/Al interfaces" S.J. Jones, A.B. Swartzlander-Franz, Y. Chen and D.L. Williamson, Mat. Res. Soc. Symp. Proc. **297**, 1049 (1993).

H. "The effects of Ar and He dilution on the microstructure of a-Si:H detected by SAXS" S.J. Jones, Y. Chen, D.L. Williamson, U. Kroll and P. Roca i Cabarrocas, J. Non-Cryst. Solids **164-66**, 131 (1993).

I. "Microstructure of a-Si:H, a-SiGe:H, and a-SiC:H Solar Cell Materials" D.L. Williamson, Y. Chen and S.J. Jones, AIP Conf. Proc. (in press, 1994).

J. "Short range order, microstructure and their correlation with light induced degradation in a-Si:H deposited at high growth rates by cathode heating technique" S. Chattopadhyay, S.N. Sharma, R. Banerjee, D.M. Bhusari, S.T. Kshirsagar, Y. Chen and D.L. Williamson, submitted to J. Appl. Phys. (1994).

K. "Microvoid, Si, H, and Al dynamics in a-Si:H/Al_2O_3/Al structures: a small-angle x-ray scattering and infrared absorption study" J. Shinar, H. Jia, R. Shinar, Y. Chen and D.L. Williamson, submitted to Phys. Rev. (1994).

L. "The relation between film microstructure, plasma chemistry and the photoelectronic quality of a-Ge:H deposited by plasma enhanced chemical vapor deposition" S.J. Jones, Y. Chen, D.L. Williamson, P. Wickboldt, D. Pang, A.E. Wetsel, W. Paul and J.H. Chen (in preparation).

M. "Optimization of wide band gap a-SiC:H p$^+$-layers" J. Daey Ouwens, R.E.I. Schropp, W.F. van der Weg and D.L. Williamson (submitted to PVSEC, 1994).

REPORT DOCUMENTATION PAGE

Public reporting burden for this collection of information is estimated to average 1 hour per response, including the time for reviewing instructions, searching existing data sources, gathering and maintaining the data needed, and completing and reviewing the collection of information. Send comments regarding this burden estimate or any other aspect of this collection of information, including suggestions for reducing this burden, to Washington Headquarters Services, Directorate for Information Operations and Reports, 1215 Jefferson Davis Highway, Suite 1204, Arlington, VA 22202-4302, and to the Office of Management and Budget, Paperwork Reduction Project (0704-0188), Washington, DC 20503.

1. AGENCY USE ONLY (Leave blank)	2. REPORT DATE July 1994	3. REPORT TYPE AND DATES COVERED Final Subcontract Report—1 February 1991 - 31 January 1994

4. TITLE AND SUBTITLE

Small-Angle X-Ray Scattering Studies of Microvoids in Amorphous-Silicon-Based Semiconductors

5. FUNDING NUMBERS

C: XG-1-10063-3

TA: PV431101

6. AUTHOR(S)

D. L. Williamson, S. J. Jones, Y. Chen

7. PERFORMING ORGANIZATION NAME(S) AND ADDRESS(ES)

Colorado School of Mines
Department of Physics
Golden, CO 80401

8. PERFORMING ORGANIZATION REPORT NUMBER

9. SPONSORING/MONITORING AGENCY NAME(S) AND ADDRESS(ES)

National Renewable Energy Laboratory
1617 Cole Blvd.
Golden, CO 80401-3393

10. SPONSORING/MONITORING AGENCY REPORT NUMBER

TP-411-6855

DE94011840

11. SUPPLEMENTARY NOTES

NREL Technical Monitor: W. Luft

12a. DISTRIBUTION/AVAILABILITY STATEMENT

12b. DISTRIBUTION CODE

UC-271

13. ABSTRACT *(Maximum 200 words)*

This report describes work performed to provide new details of the microstructure for the size scale from about 1 nm to 30 nm in high-quality hydrogenated amorphous-silicon and related alloys prepared by current state-of-the-art deposition methods as well as by new and emerging deposition technologies. The purpose of this work is to help determine the role of microvoids and other density fluctuations in controlling the opto-electronic and photovoltaic properties. The approach involved collaboration with several groups that supplied relevant systematic sets of samples and the associated opto-electronic/photovoltaic data to help address particular issues. The small-angle X-ray scattering (SAXS) technique, as developed during this project, was able to provide microstructural information with a high degree of sensitivity not available from other methods. It is particularly sensitive to microvoids or H-rich microdomains and to the presence of oriented microstructures. The latter is readily associated with columnar-type growth and can even be observed in premature stages not detectable by transmission electron microscopy. Flotation density measurements provided important complementary data. Systematic correlations demonstrated that material with more SAXS-detected microstructure has poorer opto-electronic and photovoltaic properties and increased degradation under light soaking. New results related to alloy randomness emerged from our ability to measure the diffuse scattering component of the SAXS.

14. SUBJECT TERMS

small-angle X-ray scattering ; microvoids ; amorphous silicon ; semiconductors ; photovoltaics ; solar cells

15. NUMBER OF PAGES
43

16. PRICE CODE
A03

17. SECURITY CLASSIFICATION OF REPORT Unclassified	18. SECURITY CLASSIFICATION OF THIS PAGE Unclassified	19. SECURITY CLASSIFICATION OF ABSTRACT Unclassified	20. LIMITATION OF ABSTRACT UL